NOTICE

The quality of this microform is heavily dependent upon the quality of the original thesis submitted for microfilming. Every effort has been made to ensure the highest quality of reproduction possible.

If pages are missing, contact the university which granted the degree.

Some pages may have indistinct print especially if the original pages were typed with a poor typewriter ribbon or if the university sent us an inferior photocopy.

Reproduction in full or in part of this microform is governed by the Canadian Copyright Act, R.S.C. 1970, c. C-30, and subsequent amendments.

AVIS

La qualité de cette microforme dépend grandement de la qualité de la thèse soumise au microfilmage. Nous avons tout fait pour assurer une qualité supérieure de reproduction.

S'il manque des pages, veuillez communiquer avec l'université qui a conféré le grade.

La qualité d'impression de certaines pages peut laisser à désirer, surtout si les pages originales ont été dactylographiées à l'aide d'un ruban usé ou si l'université nous a fait parvenir une photocopie de qualité inférieure.

La reproduction, même partielle, de cette microforme est soumise à la Loi canadienne sur le droit d'auteur, SRC 1970, c. C-30, et ses amendements subséquents.

Canada

THE ZEEMAN EFFECT ON NEUTRAL ACCEPTOR BOUND EXCITONS IN SILICON

by

Serguei An

B.Sc., Moscow Institute of Physics and Technology, 1992

THESIS SUBMITTED IN PARTIAL FULFILMENT OF

THE REQUIREMENTS FOR THE DEGREE OF

MASTER OF SCIENCE

in the Department

of

Physics

SIMON FRASER UNIVERSITY

JULY 1995

ISBN 0-612-06583-9

APPROVAL

Name: Serguei An

Degree: Master of Science

Title of the thesis: The Zeeman effect on neutral acceptor bound excitons in silicon

Examining Committee:

Chairman: Dr. J. R. Dahn

Dr. M.L.W. Thewalt

Senior supervisor

Dr. S.P. Watkins

Dr. R.F. Frindt

Dr. J.C. Irwin

Internal examiner

Date approved: July 28, 1995

PARTIAL COPYRIGHT LICENSE

I hereby grant to Simon Fraser University the right to lend my thesis, project or extended essay (the title of which is shown below) to users of the Simon Fraser University Library, and to make partial or single copies only for such users or in response to a request from the library of any other university, or other educational institution, on its own behalf or for one of its users. I further agree that permission for multiple copying of this work for scholarly purposes may be granted by me or the Dean of Graduate Studies. It is understood that copying or publication of this work for financial gain shall not be allowed without my written permission.

Title of Thesis/Project/Extended Essay

The Zeeman effect on neutral acceptor bound excitons in Silicon

Author: _____
(signature)

_____
(name)

August 4th, 1995
(date)

Abstract

A Fourier Transform Michelson interferometer was used to investigate the photoluminescence of shallow acceptor-bound exciton complexes (A^0X) in Si. This technique allows for the collection of ultra high (0.03 cm^{-1}) resolution spectra with a high signal to noise ratio, thus providing the experimental tool required to study the fine structure of acceptor bound excitons in Si. Spectra were collected from crystalline Si doped with either In, Ga, Al or Tl. The effect of a magnetic field on acceptor bound excitons was studied experimentally and theoretically to determine the parameters of the valley-orbit splitting for Al, Ga and In A^0X's and the spin-orbit coupling in the In^0X. In this work we have determined the g-factors and diamagnetic shift constants and explained the diamagnetic splitting of A^0X energy levels.

ACKNOWLEDGEMENT

I would like to thank my senior supervisor, Dr. Thewalt, and Dr. Karasuyk for their invaluable guidance and support throughout this work. Special thanks to all members of the group for sharing their knowledge and creating exciting and enjoyable work environment.

Financial support from Dr. Thewalt and Simon Fraser University is gratefully acknowledged.

TABLE OF CONTENTS

LIST OF FIGURES

LIST OF TABLES

Table Page

A list of abbreviations:

A^0- neutral acceptor

A^0X- neutral acceptor bound exciton

Al^0X- neutral Al bound exciton

B^0X- neutral boron bound exciton

Ga^0X- neutral Ga bound exciton

In^0X- neutral In bound exciton

Tl^0X- neutral Tl bound exciton

BE- bound exciton

BMEC- bound multi-exciton complex

CCP- central cell potential

D^0- neutral donor

D^0X- neutral donor bound exciton

EMA- Effective mass approximation

EMT- Effective mass theory

FE- free exciton

FTS- Fourier Transform Spectroscopy

NP- no-phonon

PL- photoluminescence

SM- Shell model

VOS- valley-orbit splitting

VO- valley-orbit

Chapter 1.

1.1 Introduction.

Si is the most popular semiconductor material for industrial device production. Impurities can strongly effect the electrical properties of Si, thus, it is important to control their concentration and to understand their electronic structure. Extensive experimental and theoretical studies have been undertaken to this end. Many experimental techniques [2] were developed to investigate the energy spectrum of impurities in Si including Fourier Transform Spectroscopy (FTS). Based on the Michelson interferometer, this technique lends itself to both absorption and photoluminescence studies [2]. In this work, the combination of FTS and magnetoluminescence was used to study the fine structure of the neutral acceptor-bound exciton (A^0X) in Si. FTS can provide much higher resolution and throughput than spectroscopy based on conventional grating spectrometers. FTS will be described in more detail in the third chapter. A brief description of magnetoluminescence is given in the following section, followed by the description of the electronic levels relevant to this method.

1.2. Magnetophotoluminescence spectroscopy.

Using a laser as an excitation source, electrons in the Si are excited from the valence band to the conduction band thus creating non-equilibrium concentration of electron-hole pairs. An electron and a

hole can then recombine with the emission of a photon. This process is called radiative recombination. The photon energy of a purely electronic transition is determined by the energy of the initial and final states of the electron, as follows,

$$h\nu_{photon} = E_{initial} - E_{final} \quad (1)$$

By measuring the photon energy it is possible to determine the energy levels involved in this process.

Si has a valence band maximum at the centre of the Brillouin zone (k=0), and six equivalent conduction band minima near the boundary of the Brillouin zone along <001> directions. Indirect optical transitions from the conduction band minima into the valence band maximum thus require a third particle to satisfy the quasi-momentum conservation. This particle can be a phonon, in which case the process is called a phonon assisted transition. Following the energy conservation law, the photon energy for the usual case of phonon emission is given as

$$h\nu_{photon} = E_{initial} - E_{final} - h\Omega_{phonon} \quad (2)$$

In the case of A^0X, no-phonon recombination is possible due to the coupling of the hole with the acceptor central cell potential (CCP). The central cell potential describes impurity dependant correction to Coulomb potential and takes into account local strain field, charge redistribution and differences between the impurity and host core potentials. In this case the photon energy is simply defined by equation (1)

To obtain more information about the symmetry properties and degeneracies of the electron and hole states in A^0X one can apply external perturbations, like electric and magnetic fields or mechanical stress. When a magnetic field is applied as the external perturbation the method is referred to as magnetoPL spectroscopy.

1.3 The effective mass approximation and Shell Model.

The effective mass approximation (EMA) was initially developed to describe the behaviour of free charge carriers in semiconductors and was later applied to explain free excitons (FE) and shallow impurity centres. A basis statement of the EMA is that free charged carriers in a lattice can be described as charged particles of effective mass m^*, different from mass m in free space. One of the systems that can be described by the EMA is that of a neutral donor (D^0). The D^0 complex consists of an ionized group V atom replacing a Si atom and an electron bound to it by Coulomb interaction. Under the assumption that only long range potentials are significant, the EMA uses the hydrogen atom analogy to explain this system. Hence the energy levels of the D^0 are described by a formula similar to that for the electronic energy levels of a hydrogen atom

$$E_n = -m_e^* e^4/2h^2\varepsilon^2 n^2 \quad where\ n = 1, 2, 3, ... \qquad (3)$$

where m_e^* is the electron effective mass. Further studies led to the discovery of excitons bound to neutral impurities predicted by Lampert in 1958 [3] and observed by Haynes in 1960 [4]. It was also found that

neutral impurities can trap more then one exciton [6, 28, 27]. In 1977 Kirczenow [5] proposed the Shell Model (SM) of the bound multi-exciton complex (BMEC) which can be applied to describe bound excitons as well. It explained all of the experimental results available at this time [24,25,15,16]. The SM took into consideration the symmetry of the local impurity field and the structure of the conduction and valence bands to explicitly form electron and hole wavefunctions as an antisymmetric product of single-particle wavefunctions having the symmetry properties of shallow donor states for electrons and shallow acceptor states for holes. The EM approximation and the SM will be described in more detail in the next chapter.

1.2 Motivation for this study.

The original SM did not take into account electron-electron, hole-hole and electron-hole interactions. It was also assumed that the valley-orbit splitting (VOS) due to the inter-valley scattering of the electron among conduction band minima is negligibly small for the acceptor bound exciton (BE) and BMEC. But, as early as 1977, Parsons [18] using a scanning Fabry-Perot interferometer presented evidence of extra fine structure in the PL spectra of phosphorus BMEC's that could be explained only in terms of inter-particle interactions. This inspired further studies of acceptor BE and BMEC [19,20,22]. In 1978, Elliot, Smith and McGill detected VOS in the A^0X spectra of Si doped with Al. The VOS in boron bound exciton was discovered by Karasuyk et al. in

1983 [35]. Unexpected additional structure was resolved in high resolution spectra of Al, Ga and In BE's by Thewalt et al. [17] in 1990. The high resolution FTS studies of the boron BE under stress and magnetic field performed by Karasuyk et al. [9, 39] explained the details of inter-particle interactions in B^0X and determined the order of the valley-orbit energy levels. The experiments by Thewalt [17] and Karasuyk [9,39] inspired the further Zeeman studies of group III A^0X's in Si presented in this thesis.

Chapter 2. The structure of A^0 and A^0X in a magnetic field.

2.1 The effective mass theory of shallow impurity centres.

The effective mass theory (EMT) was first developed to explain the results of cyclotron resonance measurements on free charge carriers in Si [36]. The motion of a free charged particle in a perfect crystal can be described by the Hamiltonian

$$H_0 = \frac{P^2}{2 \bullet m} + U_0(k) \qquad (4)$$

where $U_0(k)$ is the periodic potential and m is the mass of the particle in free space. According to the EMT the effect of the periodic potential can be accounted for by introducing the effective mass m^*, and the Hamiltonian (4) can be rewritten [36] as

$$H_0 = \frac{P^2}{2 \bullet m^*} \qquad (5)$$

In this approximation the carrier can be described as a particle of effective mass m^*. The effective mass is not a scalar anymore but a second rank tensor.

Impurities and other defects of the crystal structure can trap free electrons and/or holes into a variety of localized states. The simplest examples of such states are substitutional donors or acceptors. Let us consider an isolated group III atom replacing a Si atom in the lattice. This atom needs an extra electron to form a bond with the Si atoms, and hence, becomes a negatively charged ion. A hole can then be bound to this impurity creating a complex similar to a hydrogen atom. By assuming that 1) the host lattice forms a uniform environment with

dielectric constant ε, and 2), that a hole can be treated as a charged particle of mass m^* (hole effective mass), one can use the hydrogen atom analogy. The Hamiltonian of the system is then written as

$$H_{acceptor}=H_0+U_c(r)+V_c(r) \quad (6)$$

where $U_c(r) = e^2/\varepsilon r^2$ is the Coulomb potential and $V_c(r)$ is the Central Cell Potential (CCP) which represents the impurity-dependant correction to the Coulomb interaction. The CCP takes into account a number of effects including the local strain field, charge redistribution, differences between the impurity and host core potentials. In the effective mass approximation (EMA) ($V_c(r)=0$) the eigenvalues of the Hamiltonian are described by formula (3) following the H atom analogy. It is implied that U_c is small in comparison with the band gap and is a smooth function on a scale of the lattice constant. As a result one assumes that a hole is loosely bound to the impurity and perturbation theory can be used to form a wavefunction of the hole as a linear combination of the Bloch functions at the top of the valence band multiplied by a smooth envelope function. That is

$$\Phi_i^{hole}(r) = \sum_j a_{ij} F_j(r)\varphi_j(r) \text{ where } j;i = 1;2;3;4 \quad (7)$$

where $F_j(r)$ are the envelope functions and $\varphi_j(r)$ are the Bloch wave functions at the top of the valence band. The indexes i and j run from 1 to 4 since the top of the valence band is four-fold degenerate, hence four linearly independent functions are required to describe it. The

wavefunctions at the top of the valence band of Si form the basis of the irreducible four-fold representation Γ_8 of the point group O_h, the group of directions of the spatial group O^7_h of the pure Si crystal. The point group T_d of a substitutional impurity site in the Si lattice is a subgroup of O_h. The acceptor wavefunctions formed from the Bloch functions at the top of the valence band transform according to the Γ_8 representation of the T_d group. In the spherical approximation the states described by these functions have total angular momentum $j=3/2$ and can be classified according to the projections $m_j = \pm 1/2; \pm 3/2$ of j on an arbitrary axis. Thus, in the absence of external perturbation the acceptor ground state is a four-fold degenerate state.

2.2 Excitons bound to neutral acceptors (A^0X).

In 1958 Lampert, using the H molecule analogy, suggested that a neutral impurity and a FE could form a stable complex with a nonzero binding energy [3]. Following this suggestion Haynes in 1960 observed excitons bound to neutral donors (D^0X) and neutral acceptors (A^0X) in Si [4].

One can think of A^0X as a complex incorporating three particles, one electron and two holes, moving in the field of a negatively charged ion. According to the Shell Model, the wavefunctions of A^0X can be constructed as antisymmetrized products of single-particle wavefunctions. The single-hole wavefunctions have the same form and

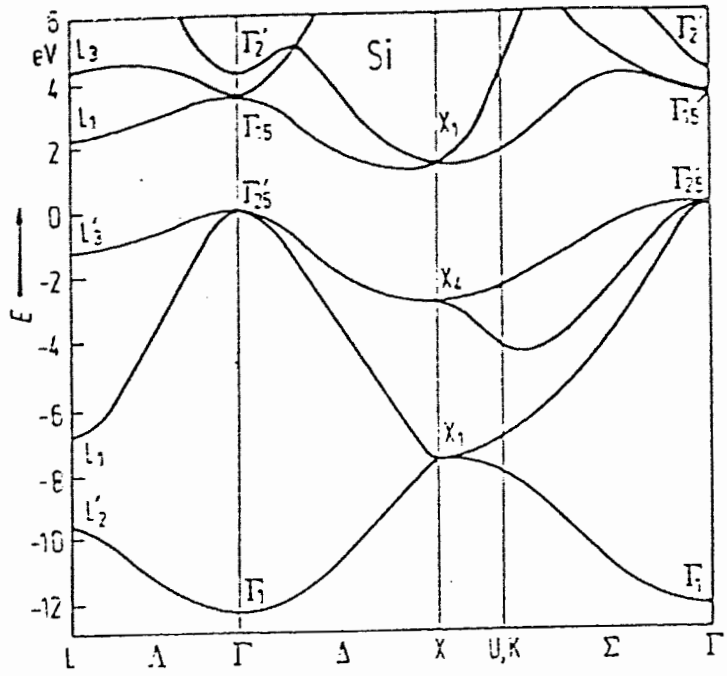

(a)

(b)

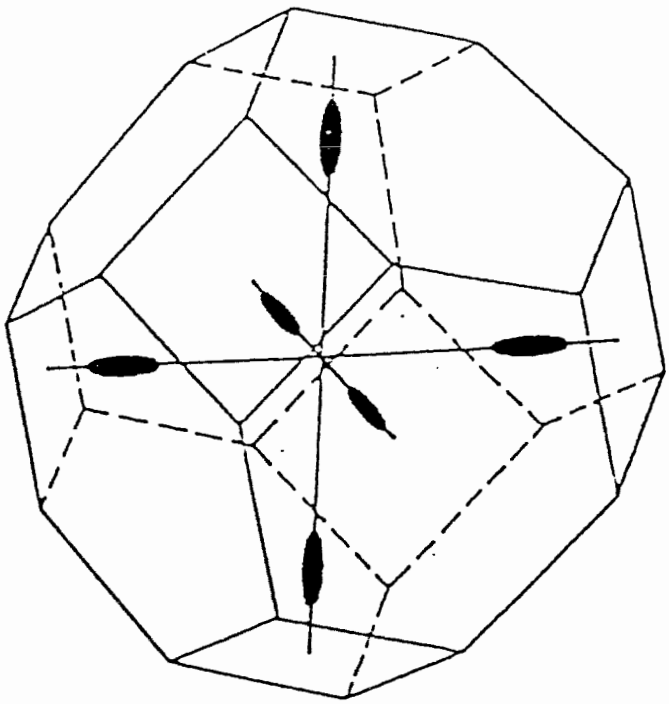

fig.1 a) Band structure of silicon (40) b) constant energy surfaces of the conduction band minima (41).

symmetry as the wave functions of a shallow A^0. The single-electron wavefunction in A^0X has the structure of the shallow donor wavefunction. Neglecting the spin-orbit interaction they can be constructed as linear combinations of the Bloch functions at the six Si conduction band minima multiplied by smooth envelope functions and a spinor function with the spin $s=1/2$.

$$\Phi_{\alpha i}(r) = \sum_j \alpha_{ij} F_j(r)\psi_j(r)\sigma_\alpha \quad where\ i;j = 1;..;6\ and\ \alpha = 1;2 \tag{8}$$

where $\Phi_i(r)$ is a spatial part, $F_j(r)$ is the envelope function, σ_α is the spin function and $\psi_j(r)$ is one of the six Bloch functions at the minimum of the conduction band. The conduction band in Si has six equivalent minima located approximately 85% of the way to the Brillouin zone boundary in the <001> directions (see fig. 2). The constant energy surfaces in k-space around each minimum are ellipses of revolution with the long axis along the <001> directions. Because there are six equivalent minima one can construct only six independent linear combinations. These six combinations can be constructed so that they form the basis of the A_1+E+T_2 irreducible representations of the T_d group. Interaction with the tetrahedral part of the impurity potential can split the energy levels of the A_1, E and T_2 states. This splitting is referred to as the valley-orbit splitting (VOS). In the basis of the single-valley functions

$$u_1=(1,0,0,0,0,0)\ (X) \tag{9}$$

$$u_2=(0,1,0,0,0,0)\ (-X) \tag{9a}$$

$u_3=(0,0,1,0,0,0)$ (Y) (9b)

$u_4=(0,0,0,1,0,0)$ (-Y) (9c)

$u_5=(0,0,0,0,1,0)$ (Z) (9d)

$u_6=(0,0,0,0,0,1)$ (-Z) (9e)

The valley-orbit wavefunctions are given by the following linear combinations

Γ_1: $\frac{1}{\sqrt{6}}(1, 1, 1, 1, 1, 1)$ (10)

Γ_3 : $\frac{1}{\sqrt{12}}(-1,-1,-1,-1,2,2)$ (11)

$\frac{1}{2}(1,1,-1,-1,0,0)$

Γ_5 : $\frac{1}{\sqrt{2}}(1,-1,0,0,0,0)$ (12)

$\frac{1}{\sqrt{2}}(0,0,1,-1,0,0)$

$\frac{1}{\sqrt{2}}(0,0,0,0,1,-1)$

2.3 A^0X and A^0 under magnetic field.

2.3.1 A^0X in a magnetic field.

In a typical PL experiment, a sample is illuminated by an external source to create non-equillibrium electron-hole population. Non-equillibrium electron and holes recombine emitting photons. The energy of the photons depends on the energy levels of the initial and final states of the optical transitions. In this particular case of interest, the initial state is A^0X and the final state is A^0. That is, $A^0X \rightarrow A^0 + photon$.

The energy levels and the eigenfunctions of A^0X in a magnetic field can be determined by diagonalizing the matrix of the Hamiltonian

$$H = H_0 + H_{hh} + H_{eh} + H_{vos} + H_{hh}(B) + H_e(B) \quad (13)$$

where H_0 is the zero order Hamiltonian without interaction among particles, H_{hh} describes the hole-hole coupling, H_{eh} is the electron-hole interaction, H_{vos} is the VOS and $H_{hh}(B)$ and $H_e(B)$ account for the interaction of the holes and the electron with magnetic field.

Following Pauli exclusion principle the symmetry of the two-hole state should have the symmetry of the antisymmetric product of the two Γ_8 states. That is, $\{\Gamma_8 X \Gamma_8\} = \Gamma_1 + \Gamma_3 + \Gamma_5$. As we found out, two holes form the spin singlet Γ_1 ground state in all A^0X's, investigated in this study. This simplifies further consideration because the Γ_1 state can not be split by any interaction. Interaction of the electron with the magnetic field can be described in the single-valley basis by the Hamiltonian [9]

$$H_e = \frac{1}{2}\mu_B g_e (B_x\sigma_x + B_y\sigma_y + B_z\sigma_z) + H^{dia}(B^2) \quad (14)$$

where g_e is the g-factor, μ_B is the Bohr magneton, B_x, B_y, B_z are the components of the magnetic field and $(\sigma_x, \sigma_y, \sigma_z)$ is the set of Pauli matrixes. The first term accounts for the paramagnetic splitting of the states according to the spin projections $m_s = \pm\frac{1}{2}$ on the direction of magnetic field. H^{dia} describes the diamagnetic shift of the energy levels and is proportional to B^2. In the single-valley basis (eq. 9a-9e) H^{dia} can be described as [9]:

$$H_{vosdia} = q_{II}^e * B^2 \cos^2(\beta) + q_{per}^e * B^2 \sin^2(\beta) \quad (15)$$

where $q_{II}{}^{e}$ and $q_{per}{}^{e}$ are the diamagnetic shift constants, and β is the angle between the direction of a magnetic field and the particular valley. If $q_{II} \neq q_{per}$ then the diamagnetic shift will depend on β. Diamagnetic constants can be different because of the strong anisotropy of the conduction band minima. For the three main orientations, diamagnetic shifts of the states derived from x, y and z-valleys will be [9] given by

B II [001]: $\Delta E_x^{dia}=\Delta E_y^{dia}=q^e_{per}B^2,\ \Delta E_z^{dia}=q^e_{II}B^2;$ (16)

BII[110]: $\Delta E_x^{dia}=\Delta E_y^{dia}=(q_{II}^e+q^e_{per})B^2/2,\ \Delta E_z^{dia}=q^e_{per}B^2;$ (17)

BII[111]: $\Delta E_x^{dia}=\Delta E_y^{dia}=\Delta E_z^{dia}=(\frac{2}{3}q^e_{per}+\frac{1}{3}q^e_{II})B^2;$ (18)

The VOS in zero field can be described by two parameters, Δ_1, equal to $E_{\Gamma_1}-E_{\Gamma_5}$ and Δ_3, equal to $E_{\Gamma_3}-E_{\Gamma_5}$. In the single-valley basis (eq. 8a-8e) the VOS matrix is of the form:

$$H_{vos}^{zero}=\begin{pmatrix} d_1 & d_1 & d_2 & d_2 & d_2 & d_2 \\ d_1 & d_1 & d_2 & d_2 & d_2 & d_2 \\ d_2 & d_2 & d_1 & d_1 & d_2 & d_2 \\ d_2 & d_2 & d_1 & d_1 & d_2 & d_2 \\ d_2 & d_2 & d_2 & d_2 & d_1 & d_1 \\ d_2 & d_2 & d_2 & d_2 & d_1 & d_1 \end{pmatrix}$$

where $d_1=(\Delta_1+2\Delta_3)/6$ and $d_2=(\Delta_1-\Delta_3)/6$. To describe VOS in a magnetic field one has to solve the eigenvalue problem for :

$H_{vos}= H^{dia}+H^{zero}{}_{vos}$ (19)

The resulting eigenfunctions are linear combinations of the single-valley functions. One can then determine phenomenological constants (g and q

factors) by comparing the theoretical transition energies with experimental results.

2.4 A^0 in a magnetic field.

As a result of the radiative recombination of an electron and a hole A^0X transforms in to A^0. A^0 is a complex of a negatively charged acceptor ion and a hole which bound to it. Thus, to describe A^0 in a magnetic field one needs to present the description of the Γ_8 hole state in a magnetic field [8].

The main assumption for constructing $H_h(B)$ is that the Hamiltonian should be invariant under the symmetry operations included in the T_d group [7]. It was found that the Hamiltonian for the hole in the Γ_8 state can be written in it's most general form[2] as:

$$H^h(B) = \mu_B[g_1(\vec{B} \bullet \vec{J}) + g_2 \Sigma B_i J_i^3] + q_1 B^2 + q_2(\vec{B} \bullet \vec{J})^2 + q_3 \Sigma B_i^2 J_i^2 \qquad (20)$$

A group-theoretical analysis of this Hamiltonian for cubic symmetry was presented by Zakharchenya and Rusanov in 1965 [30] Because T_d is the subgroup of O_h all combinations are invariant under the T_d symmetry operations as well. For the T_d symmetry this problem was solved analytically for three main orientations (<001>, <110>, <111>), by Bhattacharjee and Rodriguez in 1972 [5]. They used the following representation of the angular momentum matrices [36]:

$$J_x = \begin{pmatrix} 0 & \frac{\sqrt{3}}{2} & 0 & 0 \\ \frac{\sqrt{3}}{2} & 0 & 1 & 0 \\ 0 & 1 & 0 & -\frac{\sqrt{3}}{2} \\ 0 & 0 & -\frac{\sqrt{3}}{2} & 0 \end{pmatrix}; \; J_y = \begin{pmatrix} 0 & -\frac{\sqrt{3}}{2} & 0 & 0 \\ \frac{\sqrt{3}}{2}i & 0 & -i & 0 \\ 0 & i & 0 & -\frac{\sqrt{3}}{2} \\ 0 & 0 & \frac{\sqrt{3}}{2}i & 0 \end{pmatrix}; \quad (21)$$

$$J_z = \begin{pmatrix} \frac{3}{2} & 0 & 0 & 0 \\ 0 & \frac{1}{2} & 0 & 0 \\ 0 & 0 & -\frac{1}{2} & 0 \\ 0 & 0 & 0 & -\frac{3}{2} \end{pmatrix};$$

in the basis of the functions [36]:

$$\varphi^{(8)}_{3/2} = \frac{1}{\sqrt{2}}(X + iY)\ \alpha >; \qquad (22)$$

$$\varphi^{(8)}_{1/2} = \frac{i}{\sqrt{6}}[(X + iY)/\beta > -2Z/\alpha >];$$

$$\varphi^{(8)}_{-1/2} = \frac{1}{\sqrt{6}}[(X - iY)/\alpha > +2Z/\beta >];$$

$$\varphi^{(8)}_{-3/2} = \frac{i}{\sqrt{2}}(X - iY)/\beta >;$$

Chapter 3.

3.1 Fourier Transform Spectroscopy.

Typical A^0X binding energies for Si are about 4-12 meV, thus the temperature of the sample must be low enough to prevent thermal dissociation of the A^0X states and thermal broadening of the PL spectral lines. The standard experimental set-up for low temperature PL spectroscopy includes a cryogenic system, an excitation source, a spectrometer and a detector. As was previously mentioned, a magnetic field can be applied to lift degeneracies (the Zeeman effect) and study the symmetry properties of A^0X states. A 15T superconducting magnet was used for the Zeeman measurements in these studies.

The collection of ultra-high resolution spectra was possible because a Fourier transform spectrometer (FTS) was used. The basis for FTS is a Michelson interferometer, see fig.2. In this set-up the light from a source (ie. sample) S is collimated and directed toward a beamsplitter by a parabolic mirror. The beamsplitter divides the light into two beams, which are then reflected by mirrors M_1 and M_2. The reflected beams are re-combined at the beamsplitter and then focused on to the detector D. The mirror M_1 is fixed and the mirror M_2 is moving. The optical path difference between the two beams thus depends on the position of the moving mirror M_2. The interference conditions for different wavelengths of light change as the mirror M_2 is moving. The measured light intensity I_{out} at the detector output is related to the input intensity I_{in} by:

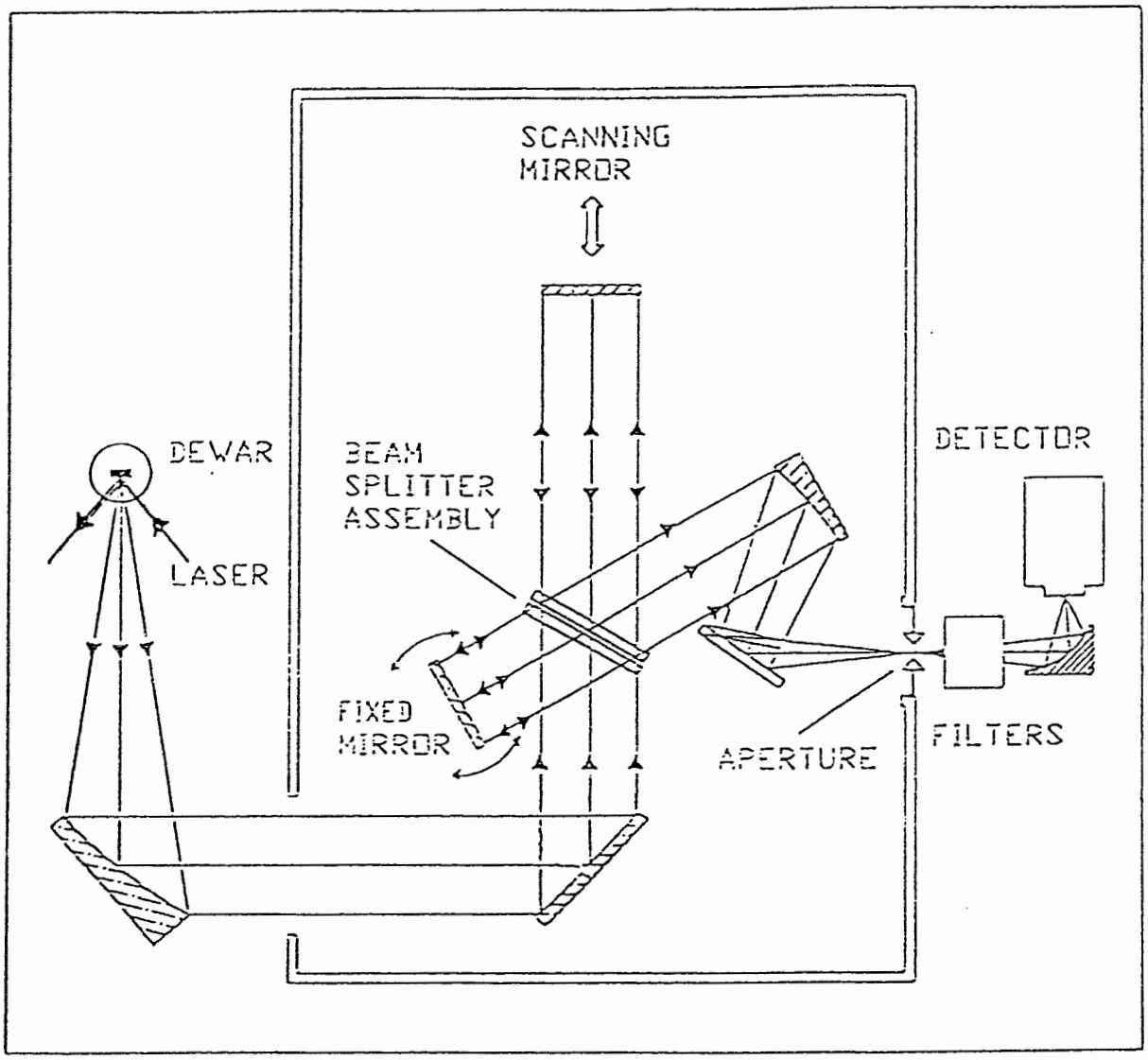

fig.2 Schematic diagram of the Michelson interferometer with dynamic alingment used in this studies. The four collimated beams incident on the beamsplitter are 1) the PL from the source, 2) from the "fixed" mirror, 3) from the scanning mirror, 4) to the detector. The orientation of the "fixed" mirror is dynamically changed in order to keep the interferometer aligned. The filter box is mounted in the detector path to use the optical filters for the light rejection.

$$I_{out} = \frac{I_{in}}{2} + \frac{1}{2}\int S(\lambda^{-1})\cos(2\pi\lambda^{-1}x)d(c\lambda^{-1}) \quad (23)$$

where x is the optical path difference. To obtain an actual energy vs. intensity spectrum we have to perform a Fourier transformation

$$S(\lambda^{-1}) = 2\int\left(I_{out} - \frac{I_{in}}{2}\right)\cos(2\pi\lambda^{-1}x)dx \quad (24)$$

In practice the scan length of the moving mirror is limited so the integral (24) has to be over some finite range, thereby, limiting the resolution of the system. The resolution of a Fourier spectrometer and the scan path length are related by the equation

$$r=0.61/L \quad (25)$$

where r is resolution and L is the length of the scanning path. Optical filters are required to prevent laser radiation from falling on the detector.

A FTS provides some advantages over a conventional grating spectrometer. The main advantage of a FTS is it's very high resolution. The resolution of a grating spectrometer is given by

$$r = \frac{\lambda}{\Delta\lambda} = mN \quad (26)$$

where N is the number of rulings in the grating, m is the order of interference and λ is the working wavelength. Thus, the theoretical limit for the resolution of the grating with 1200 rulings/mm, 10cm long in the first order of interference at the wavelength of 1100 μm is 0.08 cm^{-1}. In practice the resolution is limited by the diffraction from the entrance slit, requirements on the throughput, etc. The highest resolution of 0.4cm^{-1} in Si A^0X PL spectroscopy using grating spectrometers was achieved in

experiments by Elliot et al. [33]. The theoretical resolution of a F-T spectrometer with a path length of 0.25m is 0.02 cm^{-1} and an actual resolution of 0.03 cm^{-1} was achieved in our experiments using a BOMEM DA8 FTS.

Another important advantage of FTS is it's better signal-to-noise ratio. The maximum throughput of a Fourier spectrometer is [23] given by

$$\theta_1 = 2\pi A^I \frac{\Delta\nu}{\nu_{max}} (cm^2 sr) \tag{27}$$

where A^I is the area of the interferometer mirrors being illuminated, $\Delta\nu$ is the resolution of the spectrometer and ν_{max} is the maximum wavenumber in the spectrum. The throughput of a grating spectrometer is [23] given by

$$\theta_G = \frac{hA^G\Delta\nu}{fa\nu^2} (cm^2 sr) \tag{28}$$

where A^G is the area of the grating being illuminated, f is the focal length of the collimating mirror, h is the height of the slit, and a is the grating constant. Thus the ratio of throughputs for a Fourier vs. a grating spectrometers for the same resolution is expressed as

$$\frac{\theta_I}{\theta_G} = \frac{2\pi A^I fa\nu^2}{A^G h\nu_{max}} \tag{29}$$

This equation shows that there is a ν^2 dependence on the ratio of the throughputs. As one can see the throughput of a Fourier spectrometer is much better then that for a grating spectrometer in the near infra-red wavelength range (1-1.1μ). For a typical grating spectrometer with a focal

length f=1m, a slit height h=1cm and the above mentioned grating the ratio of the throughputs $\Theta_1:\Theta_2$ for the same resolution would be 100:1. These advantages are important for high resolution experiments.

3.2 Sample preparation and experimental procedure.

3.2.1 Sample preparation.

The samples were cut from x-ray oriented single crystals of float-zone grown silicon doped with group III acceptors in concentrations of 10^{14}-10^{15} cm^{-3}. Typical sample dimensions were 2x2x25 mm. In order to remove damaged and oxidized layers the samples were cleaned in methanol and etched in a 5:3:10 solution of concentrated HNO_3, HF and acetic acid and, finally, washed in distilled water to remove acidic residue.

3.2.2 Experimental procedure.

The samples were mounted in a stress-free manner and immersed in liquid He in the bore of the superconducting magnet. It was possible to reach temperatures below 2K by pumping on the He vapour. At these temperatures (~2.2K) liquid He becomes superfluid, thus eliminating the light scattering associated with boiling. In order to create non-equilibrium electrons and holes the sample was illuminated by a titanium sapphire laser. The laser was tuned to a wavelength of 980 nm and provided typical cw power of 700 mW. The average power density

was 2-3 W/cm^2. The sample heating due to laser radiation was negligible. The spectra were collected using an avalanche photodetector (APD). To reflect the laser radiation, we used a holographic rejection filter with a cut-off wavelength of 990 nm. These filters can be tuned to a slightly shorter wavelength by tilting. The typical resolution obtained in our experiments was 0.03-0.07 cm^{-1}. The signal was collimated by a lens and directed toward the beamsplitter by a set of flat mirrors.

Chapter 4. Experimental results and discussion.

4.1 Excitons bound to Al acceptors.

4.1.1 Experiment.

We begin our studies with Al^0X because Al is the isocoric impurity in Si, thus it should have the smallest chemical shift and other central cell effects [32]. As well, the PL spectra of Al^0X have a convenient component separation.

The Al^0X in crystalline Si was studied in magnetic fields up to 12T parallel to crystallographic axes <001>, <110>, <111>. At zero magnetic field, the aluminum BE NP PL spectrum consists of three well resolved doublets, with the same splitting in each of the doublets (fig. 3). This suggests that there are three initial and two final states or vice versa. The origin of the threefold splitting was investigated and determined in this study.

We neglected the recently discovered A^0 ground state splitting, which is responsible for the doublets, in our analysis, since it is small ($0.1cm^{-1}$) relative to other splittings, and consider the final state as a fourfold-degenerate Γ_8 state. For information about A^0 ground state studies see ref.[38].

The analysis of our data for Al in Si shows that the order of the valley-orbit states in zero magnetic field is as follows: Γ_1 is highest in energy then Γ_5 and Γ_3. Fig. 4 illustrates, schematically, the possible evolution of the valley-orbit (VO) electronic states in a magnetic field. In

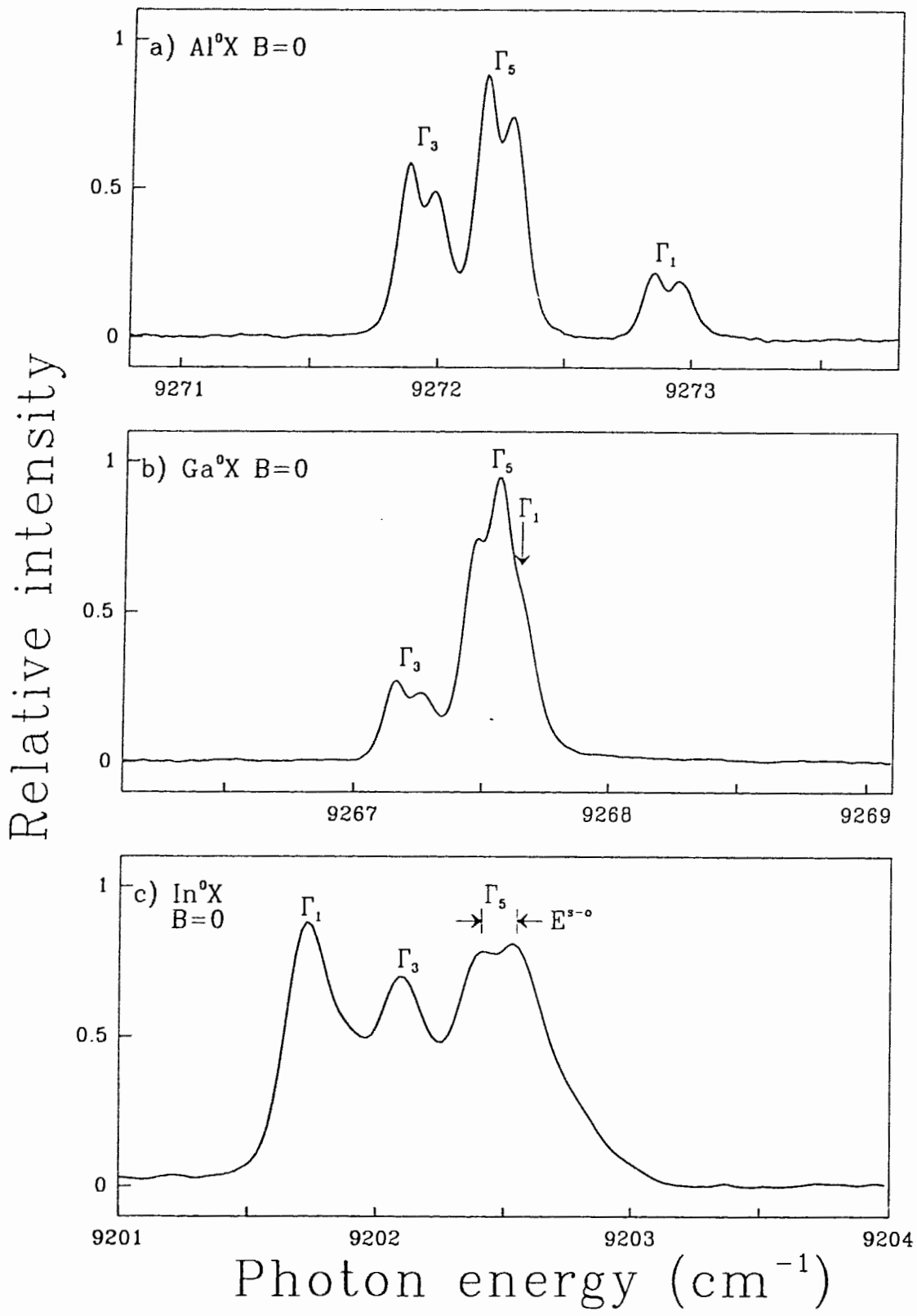

fig.3 The spectra of no-phonon PL : a) Al^0X, b) Ga^0X, c) In^0X in zero magnetic field.

a magnetic field along <001> and <110> directions the diamagnetic respond of the z conduction band minima is different from x and y ones. Thus three initial VO states (see fig. 4a) split into five due to the diamagnetic interaction (see fig. 4c). If a magnetic field is along the <111> direction than all conduction band minima are in equivalent positions and conduction band does not split. In every VO state the electron can have one of the two projections of the spin on the direction of a magnetic field ($m_s = \pm\frac{1}{2}$). The A^0 ground state splits into four in a magnetic field. Taking into account the ΔL=-1;0;1 selection rule there are six possible transitions between some VO A^0X state and the A^0 ground state in a magnetic field. Thus one would expect in a perfectly resolved spectrum to have six groups containing five/three (five for <001> and <110> and three for <111>) peaks each if all levels were populated.

The spectra were collected in Voigt configuration when the direction of magnetic field is perpendicular to the direction of a magnetic field. Upon increasing the magnetic field the components thermalize very quickly. As a result, the transitions from the states with the spin m_s=+1/2 cannot be observed in magnetic fields of moderate or high intensity (Fig. 5(B~3T Al <001>, 110, 111)) . In a strong magnetic field (fig 6) one can identify three groups containing four (for <001> & <110>) or three (for <111>) peaks each. Each group corresponds to recombination between an electron in the lower paramagnetic state (m_e=-1/2) and a hole in the states (m_j=-3/2; -1/2; 1/2) (fig. 4b). The transitions to the m_j=3/2

fig.4 a) schematic representation of A^0X and A^0 energy levels in the EMA on the left, and EMA plus tetrahedral correction on the right, b) possible optical transitions between A^0X and A^0 in magnetic field based on the $\Delta m=1;0;-1$ selection rule, where Γ_i is the A^0X VO state, m_s is the electron spin projection on the direction of magnetic field, m_j is the hole angular momentum projection on the direction of magnetic field c) the expected evolution of the valley-orbit states in magnetic field along <001> and <110> crystallographic directions.

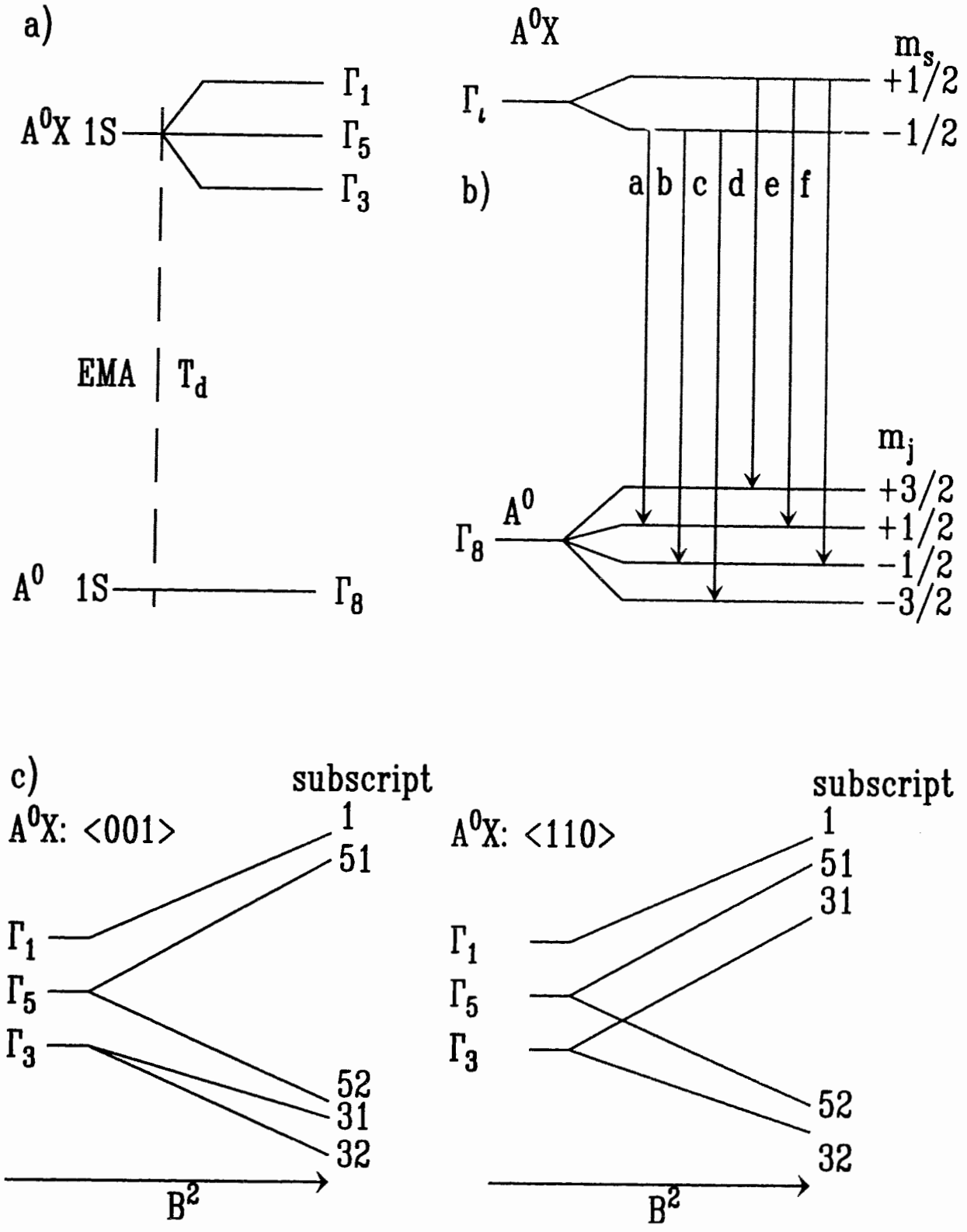
a)
A^0X 1S
Γ_1
Γ_5
Γ_3
EMA
T_d
A^0 1S
Γ_8
A^0X
m_s
Γ_i
+1/2
−1/2
b)
a b c d e f
m_j
A^0
Γ_8
+3/2
+1/2
−1/2
−3/2
c)
A^0X: <001>
subscript
1
51
Γ_1
Γ_5
Γ_3
52
31
32
B^2
A^0X: <110>
subscript
1
51
31
Γ_1
Γ_5
Γ_3
52
32
B^2

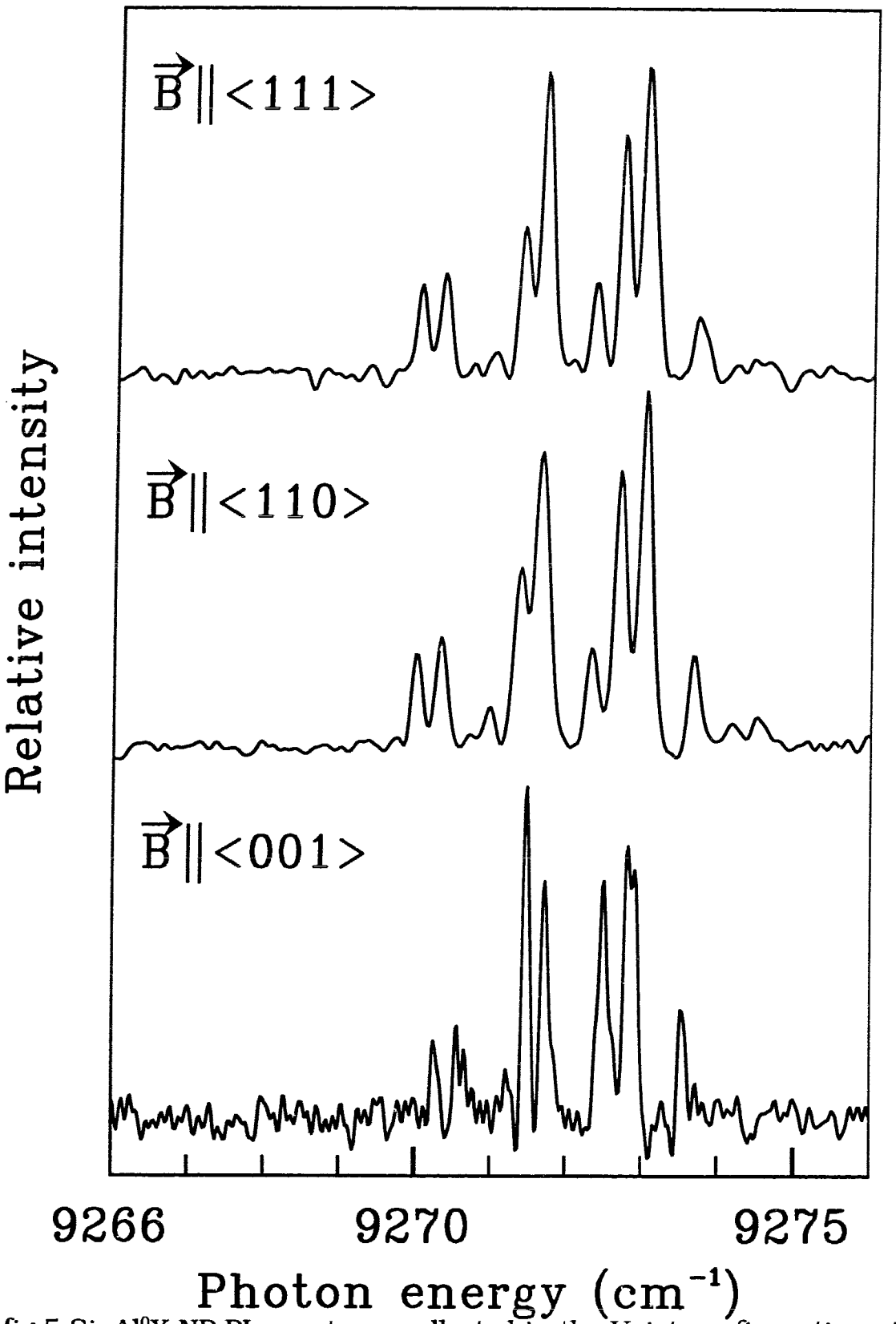

fig.5 Si: Al^0X NP PL spectrum collected in the Voigt configuration at T=2K in magnetic field B~3T for <111>, <110>, <001> orientations.

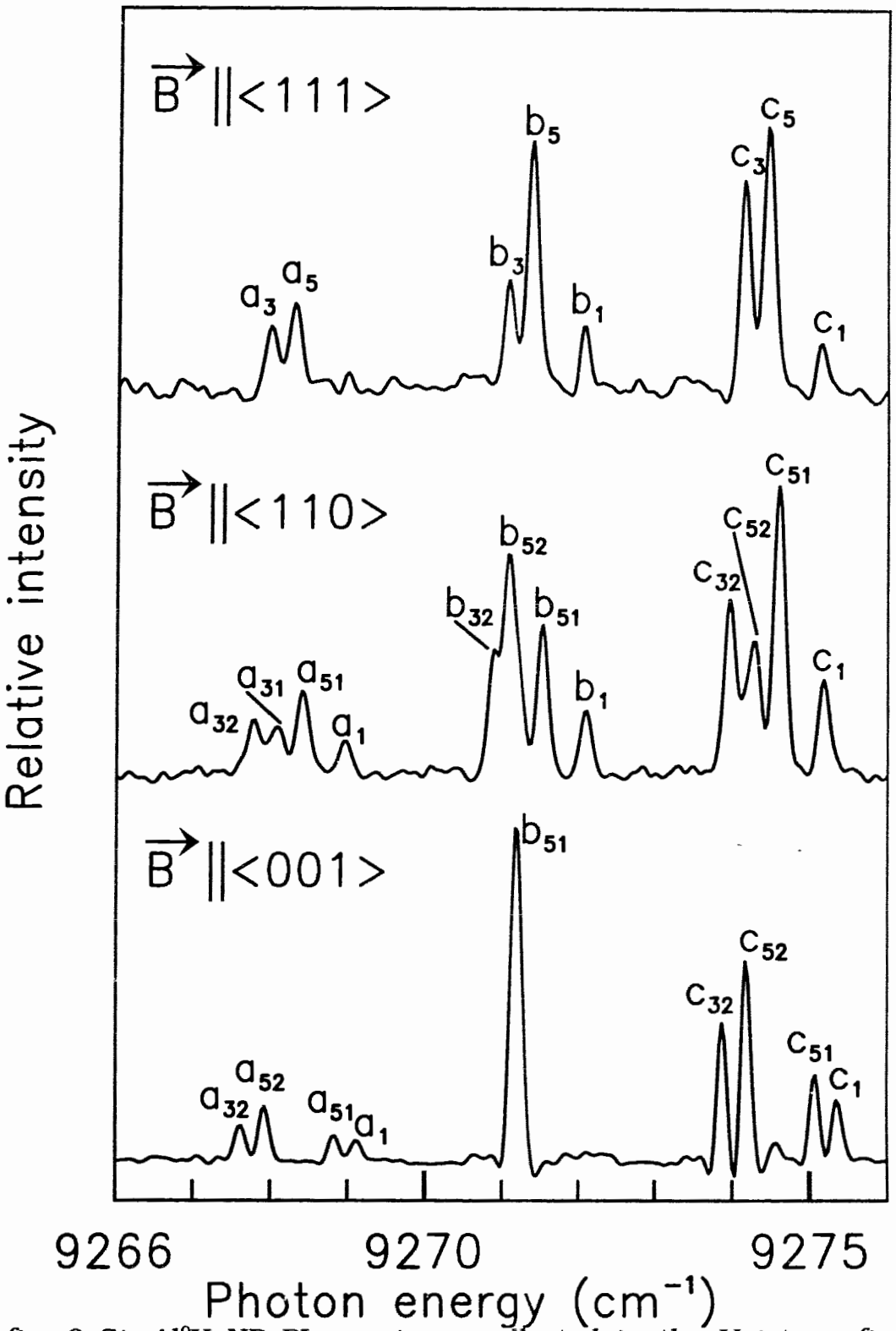

fig. 6 Si: Al^0X NP PL spectrum collected in the Voigt configuration at T=2K in magnetic field B=7T for <111>, <110> & <001> orientations. letters mark the allowed transitions according fig. 4b , the subscripts label the A^0X valley-orbit states according fig.4c

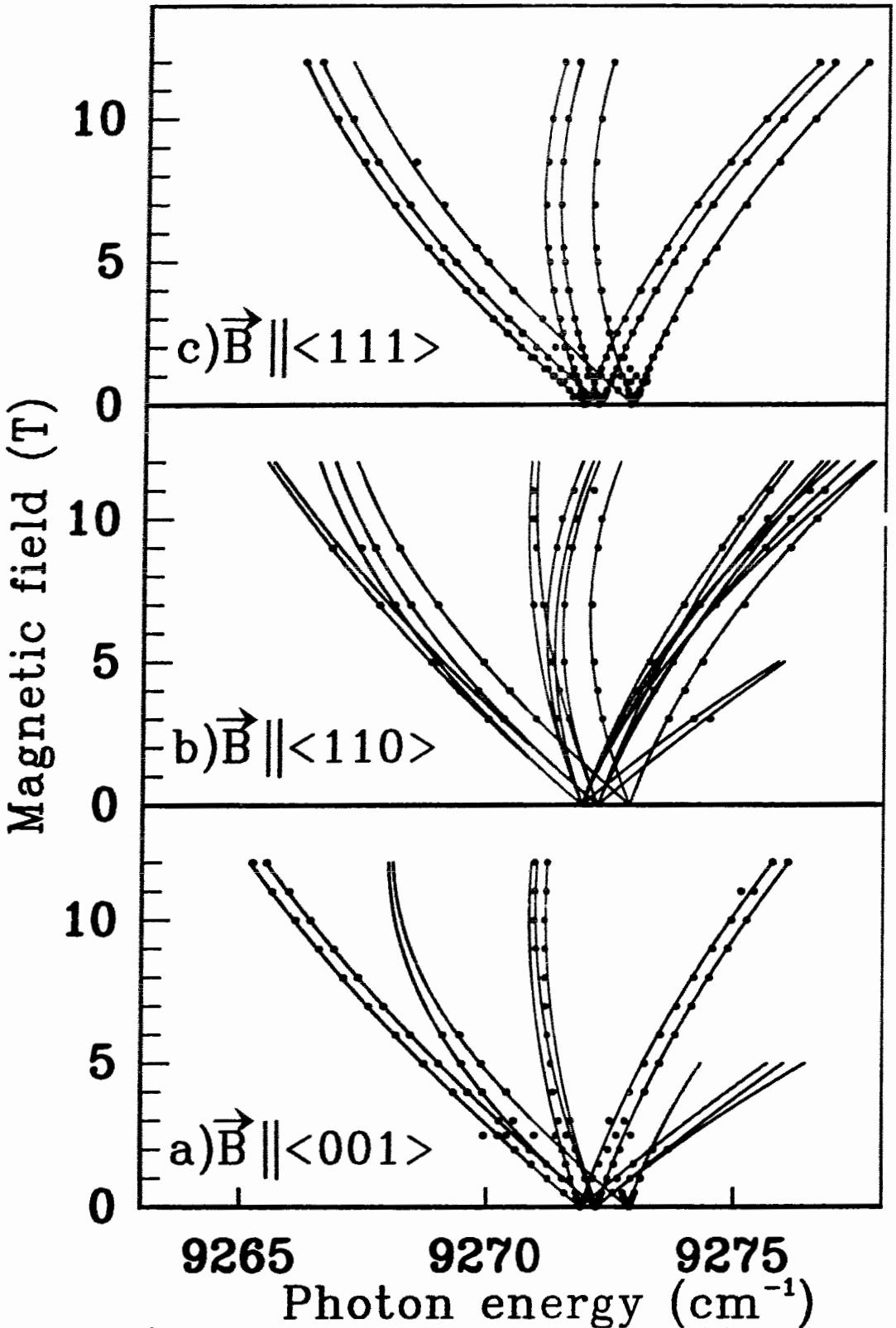

fig.7 Si: Al^0X. Experimental (circles) and theoretical (solid lines) positions of the PL peaks as a function of magnetic field with a) <001> , b) <110> and c) <111> orientations for Al^0X.

state are prohibited by the selection rule Δm=-1;0;1. Different peaks in each group correspond to different VO states of the electron in A^0X. The optical transitions in fig.6 have been labelled according to the following scheme. Letters correspond to transitions involving different combinations of angular momentum projections m_s^e and m_j^h (fig. 4b). Subscripts correspond to transitions from different valley orbit states of the electron in A^0X (fig. 4c). We were not able to detect the 3-2 components (see fig.3) for <001> and <110> directions which is consistent with selection rules calculated by Kaminskii et al [22] and Karasuyk (to be published).

Transition energies of the components versus magnetic field B for the three main orientations <001>, <110>, <111> are shown on Fig. 6 with circles. The solid lines represent the theoretical predictions discussed later.

4.1.2 Results of calculations.

We have used the same Hamiltonian to describe all A^0X studied here because they are all shallow and the holes in all A^0X form spin singlet in the ground A^0X state. The VOS was measured from the zero field spectrum and the ordering of the VO states was determined from the pattern of the VOS's in a magnetic field. The energy levels of the A^0 were calculated according to the formula [8]

$$E_{\mu}^{(8)} = \mu_B(g_1\mu + g_2\mu^3)B + [q_1 + (q_2 + q_3)\mu]B^2;\ \mu = +\tfrac{3}{2}; +\tfrac{1}{2}; -\tfrac{1}{2}; -\tfrac{3}{2} \qquad (22)$$

for the <001> direction and

$$E^{(8)}_{\pm 3/2} = \{\pm[(\tfrac{3}{2}p + \tfrac{23}{8})^2 + \tfrac{1}{2}]^{1/2} + (s_1 + \tfrac{9}{4}s_2 + \tfrac{5}{4}s_3)B\}\mu_B g_2 B;\ \text{and} \qquad (23)$$

$$E^{(8)}_{\pm 1/2} = [\pm(\tfrac{1}{2}p + \tfrac{13}{8}) + (s_1 + \tfrac{1}{4}s_2 + \tfrac{5}{4}s_3)B]\mu_B g_2 B;\ p = g_1/g_2; s_i = q_i/\mu_B g_2;$$

for the <111> direction, obtained from diagonalization of the Hamiltonian (21). The parameters g_1, g_2, q_1, q_2 and q_3 were determined from the best fit to the experiment for the directions <001> and <111>. The energy levels for the <110> direction were calculated without any adjustable parameters according to Bhachattarje and Rodriguez [8 eq.56 (a-d)]. The A^0X energy levels were found using the Hamiltonian (14).

The electron g_e-factor was fixed at a value of 2 (we have performed fitting with g_e, as an adjustable parameter, and found that it's value is 2 within 1% of accuracy). In a matrix form the Hamiltonian of VOS in a magnetic field for the <001> direction can be represented in the Γ_1, Γ_3 and Γ_5 wave function basis (see chap.2.2, 9-12) as

$$H^{dia}_{vos} = \begin{pmatrix} -\frac{2}{3}dif + \Delta_1 & \frac{\sqrt{2}}{3}dif & 0 & 0 & 0 & 0 \\ \frac{\sqrt{2}}{3}dif & -\frac{1}{3}dif + \Delta_2 & 0 & 0 & 0 & 0 \\ 0 & 0 & -dif + \Delta_2 & 0 & 0 & 0 \\ 0 & 0 & 0 & -dif & 0 & 0 \\ 0 & 0 & 0 & 0 & -dif & 0 \\ 0 & 0 & 0 & 0 & 0 & 0 \end{pmatrix};\ dif = (q^e_{II} - q^e_{per})B^2$$

if one considers the upper Γ_5 level in magnetic field as a zero level. Here Δ_1 is equal to $E_{\Gamma_1} - E_{\Gamma_5}$ and Δ_2 is equal to $E_{\Gamma_3} - E_{\Gamma_5}$ in zero field while q^e_{per} and q^e_{II} are the diamagnetic shift coefficients. The energy levels of the A^0X in a magnetic field are equal to eigenvalues of this matrix which can be found as the roots of the secular equation

$$det\,(H - \alpha I) = 0 \qquad (24)$$

where α is an eigenvalue, and I is the unit matrix. The Γ_5 states do not mix with the Γ_3, Γ_1 states since the corresponding submatrix has a diagonal form. The submatrix for the Γ_5 level has a diagonal form because in this approximation the Γ_5 wave functions are the combinations of x or y or z valleys only. The eigenvalues for the Γ_5 level are equal to the diagonal elements of the corresponding submatrix. One of the Γ_3 states also has only a diagonal element because this Γ_3 state can be chosen as a combination of X, -X, Y, -Y valleys only. This state will not be altered by magnetic fields with the <001>orientations. The remaining Γ_3 state will be mixed with the Γ_1 state in the <001> and <110> orientations of magnetic field. The energy levels for these states for the <001> direction can be found from the diagonalization of the 2X2 matrix.

$$\begin{pmatrix} -\frac{2}{3}dif + \Delta_1 & \frac{\sqrt{2}}{3}dif \\ \frac{\sqrt{2}}{3}dif & -\frac{1}{3}dif + \Delta_2 \end{pmatrix} \quad where\ dif = (q^e_{II} - q^e_{per})B^2$$

The eigenvalues of this matrix are

$$E_{1,2} = [3(dif + \Delta_1 + \Delta_2) \pm \sqrt{9dif^2 + 6dif\Delta_1 - 6dif\Delta_2 + 9(\Delta_1 - \Delta_2)^2}\,]/2; \qquad (25)$$

The theoretical transition energies equal to the differences of A^0X and A^0 energy levels are shown by the solid curves on fig.6 and the parameters are listed in Table 1. In Table 1 the parameter q_{sum} equals to

$$q_{sum} = q^{hh} + q^e - q^h \qquad (26)$$

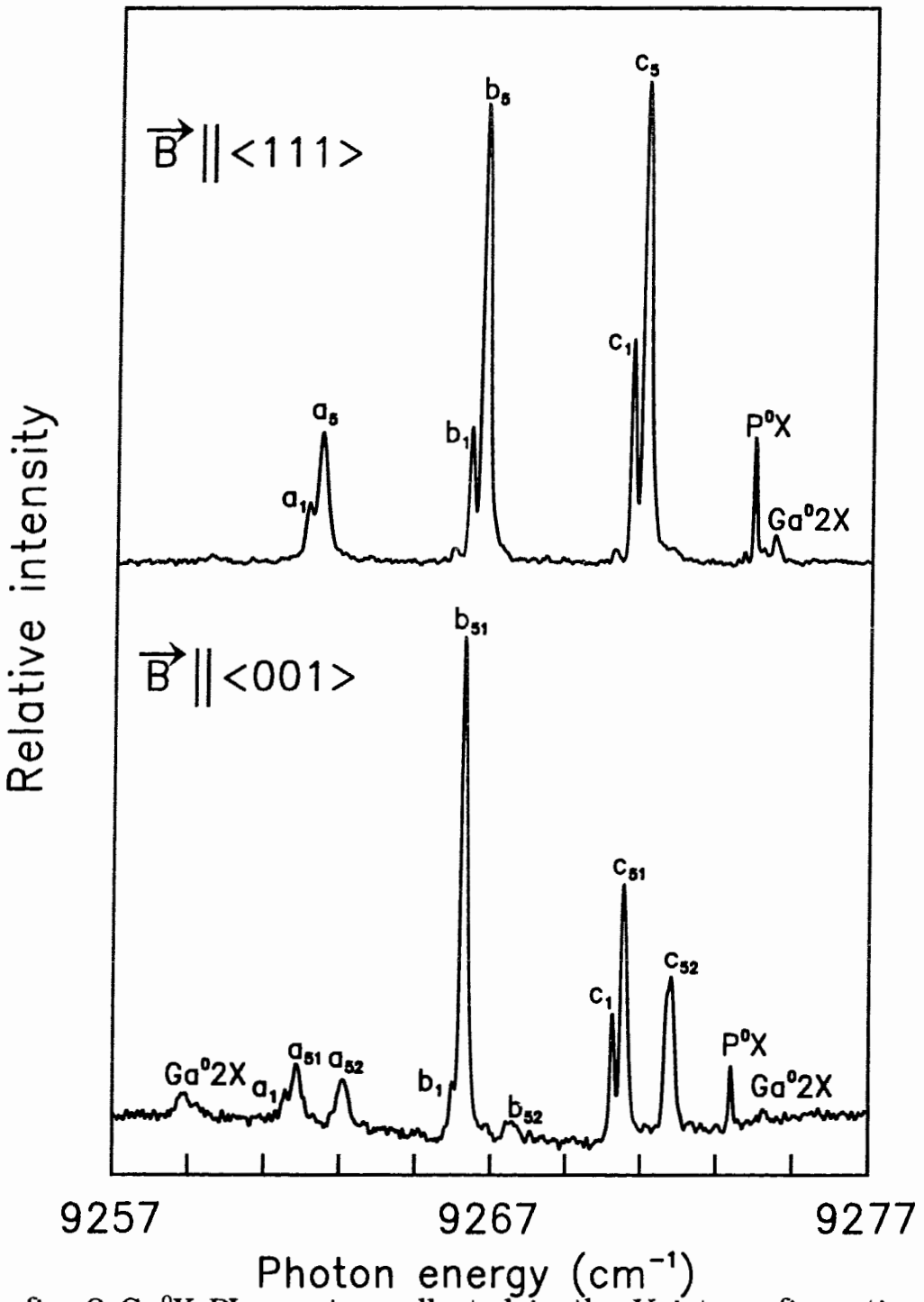

fig. 8 Ga^0X PL spectra collected in the Voigt configuration at T=2K in magnetic field B=10T for <111> & <001> orientations. letters mark the allowed transition according fig. 4b, the subscripts label the A^0X valley-orbit states according fig.4c. P^0X is a neutral phosphorus bound exciton. Ga^02X is a neutral galluim bound bi-exciton.

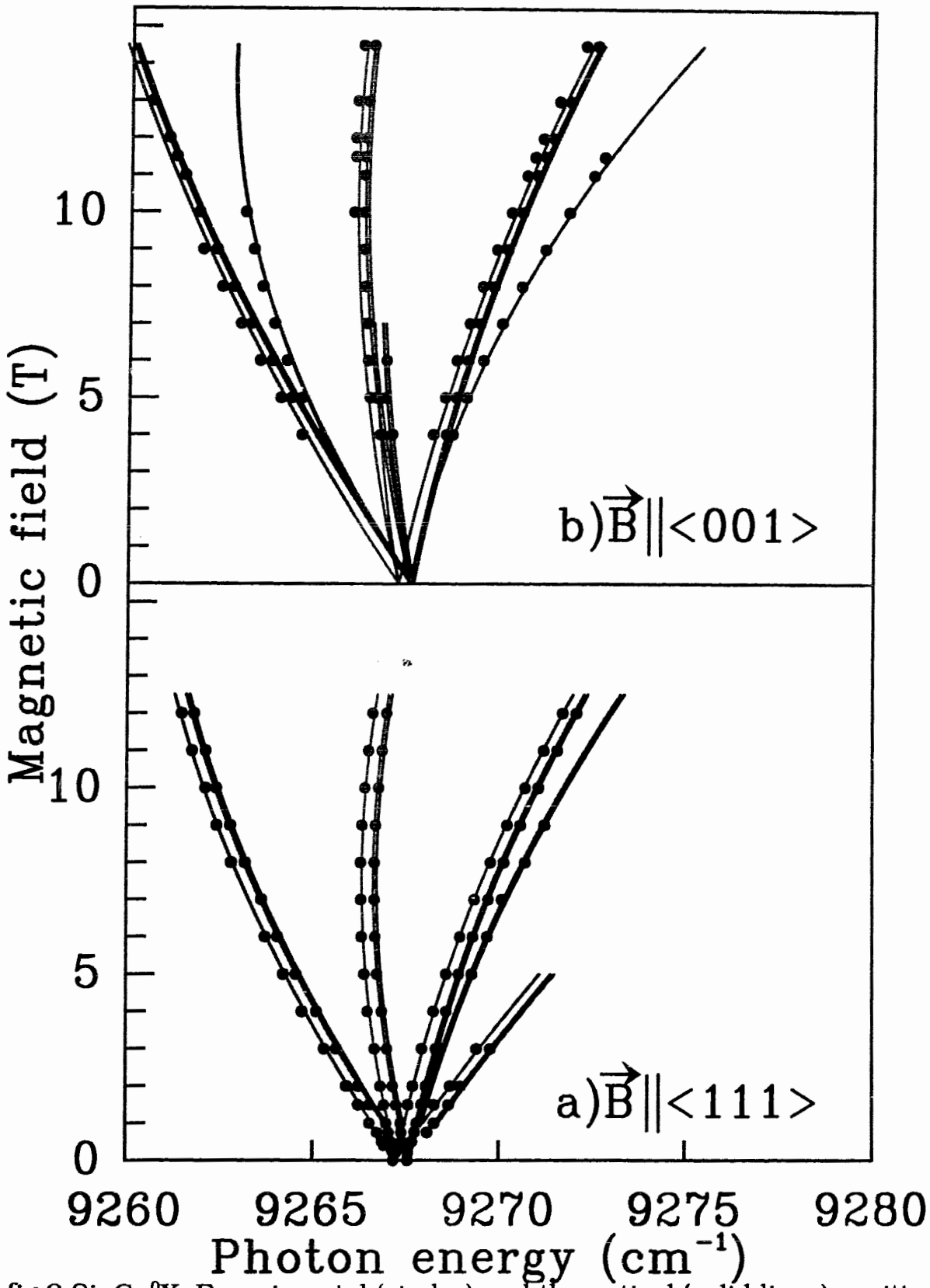

fig.9 Si: Ga^0X. Experimental (circles) and theoretical (solid lines) positions of the PL peaks as a function of magnetic field with a) <111> b) <001> orientations for Ga^0X.

here q^{hh} equals to the isotropic diamagnetic shift of the two-hole Γ_1 state, q^c is the isotropic diamagnetic shift of the electron and q^h is the isotropic diamagnetic shift of the final single hole state. Good agreement between the experimental data and the theory validates our initial assumptions about the ordering of the VO states.

4.2 Excitons bound to Ga acceptors.

In the case of the Ga A^0X, the measurement of the VOS was more complicated than for Al because the linewidth was comparable to the valley-orbit splitting between the Γ_3 and Γ_5 states and the splitting in the ground state of A^0 (see fig. 3). From PL polarization measurements for Ga^0X in a magnetic field (to be published) we determined that the order of the VO states increasing in energy is Γ_3, Γ_5 and Γ_1. The Γ_1 level is lying deeper than in the Al^0X case and separated from the Γ_5 level by only Δ_1=0.10cm^{-1}. The VOS between the Γ_5 and Γ_3 VO states of Δ_3=0.30cm^{-1} is almost the same as for the Al^0X case. We used the same labelling scheme as for the Al acceptor to classify transition energies in high magnetic fields (fig. 8). We have determined g-factors, VOS and diamagnetic shift constants from the best fit between experimental and theoretical energy transitions in magnetic fields with <001> and <111> directions. The results are shown in fig. 9 and presented in Table 1. On fig. 9 the solid curves represent the results of the theoretical prediction. Good

agreement between the experimental data and the theoretical prediction proved that our assumptions were correct.

4.3 Excitons bound to In acceptors.

As was previously mentioned, we used the same Hamiltonian to describe all A^0X. The order of the VO states had to be determined from the pattern of the Zeeman spectra and the zero field spectrum. The zero field In^0X spectrum has four clearly resolved peaks (fig. 3). The extra peak can not be explained in terms of the A^0 ground state splitting neglected in this study (for details see ref. 31). To explain the In^0X zero field spectrum we had to take into account the electron spin-orbit interaction. Components of the electron spin transform according to the Γ_6 irreducible representation of the T_d group. Since the antisymmetric products $\{\Gamma_1 x \Gamma_6\}=\Gamma_6$ and $\{\Gamma_3 x \Gamma_6\}=\Gamma_8$ contain only one irreducible representation, the spin-orbit coupling does not split these VO states. On the other hand, $\{\Gamma_5 x \Gamma_6\}=\Gamma_7+\Gamma_8$ thus the spin-orbit coupling can split the Γ_5 valley-orbit state into a doublet. The originally six-fold degenerate Γ_5 state (including spin) is split into the two-fold degenerate Γ_7 state and the four-fold degenerate Γ_8 state. The spin-orbit coupling can be described by the Hamiltonian [36]

$$H = \frac{1}{4m^2c^2}(\vec{S} X \nabla V) \bullet \vec{p}; \qquad (26)$$

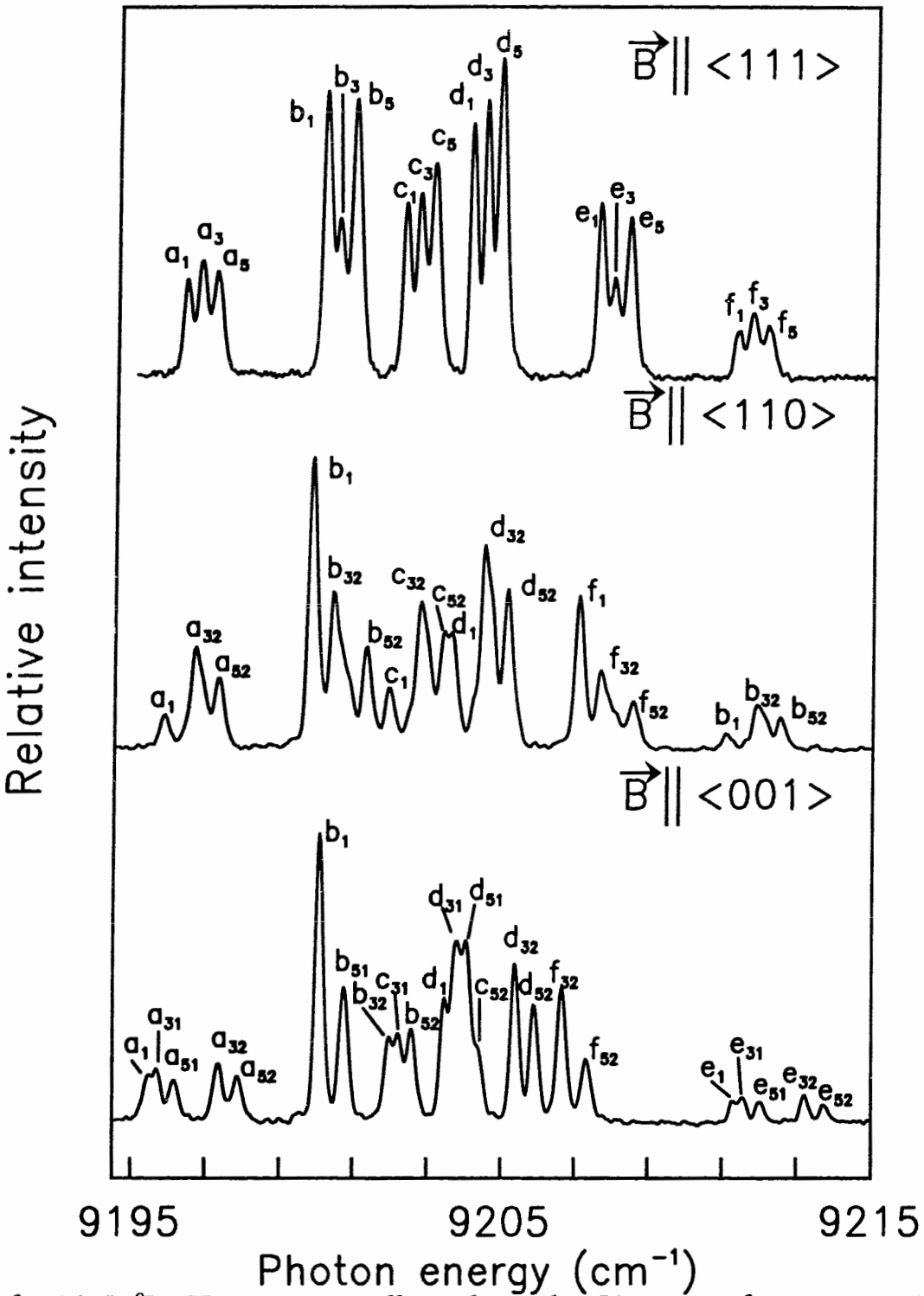

fig.10 In^{0}X PL spectra collected in the Voigt configuration at T=2K in magnetic field B=10T for <111>,<110> and <001> orientations. Letters mark the allowed transition acording fig. 4b, the subscripts label the A^{0}X valley-orbit states, according fig.4c

where $\vec{S}$ is the spin operator, V is the potential energy and $\vec{p}$ is the electronic quasi-momentum. The matrix of this Hamiltonian can be built using the method of invariants [7] in the basis

$\varphi_1=Y_1^1\alpha$; $\varphi_2=Y_1^1\beta$; $\varphi_3=Y_1^0\alpha$; $\varphi_4=Y_1^0\beta$; $\varphi_5=Y_1^{-1}\alpha$; $\varphi_6=Y_1^{-1}\beta$; (27)

here Y_1^1, Y_1^0, Y_1^{-1} have the same symmetry properties as the wavefunctions of the L=1 angular momentum; α and β are the basis functions of the spin s=1/2. Based on the symmetry properties the following Hamiltonian can be used to describe the spin-orbit interaction in T_d symmetry:

$$H = \lambda \bullet (I_x\sigma_x + I_y\sigma_y + I_z\sigma_z) \quad (28)$$

where I_x, I_y, I_z are the 3x3 matrixes of the I=1 angular momentum, σ_x, σ_y, σ_z are the Pauli matrixes and λ is the interaction constant. The wavefunctions of I=1 can be formed as linear combinations of Γ_5 basis wavefunctions. If the magnetic field is parallel to the <001> direction then the wavefunctions of I=1 can be written as

$$Y_1^1 = \tfrac{1}{2}(1,-1,i,-i,0,0); \quad (29)$$

$$Y_1^0 = -\tfrac{1}{2}(0,0,0,0,1,-1); \text{ and}$$

$$Y_1^{-1} = \tfrac{1}{2}(1,-1,-i,i,0,0);$$

The spin-orbit coupling mixes the Γ_5 VO states and the Γ_6 spin states from the two states that can be described as the I_1=3/2 (Γ_8) state and the I_2=1/2 (Γ_7) state with the energy separation of $3/2\lambda$ in zero field. Our analysis shows that the order of the valley-orbit states decreasing in

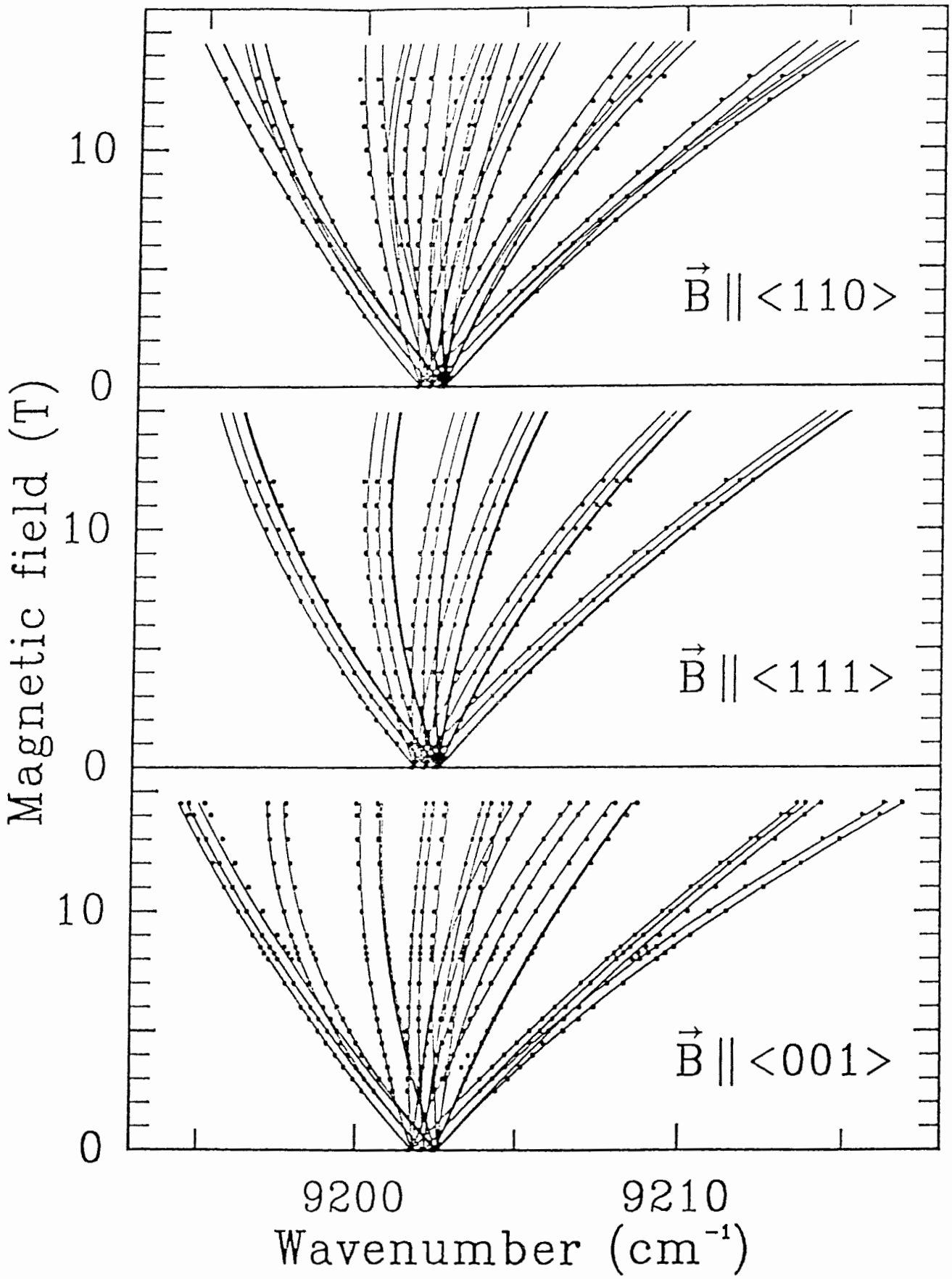

fig. 11 Si: In^0X. Experimental (circles) and theoretical (solid lines) positions of the PL peaks as a function of magnetic field with a) <001> , b) <110> and c) <111> orientations for In^0X.

energy is the following: Γ_5, Γ_3 and Γ_1. Unlike the case for Al^0X and Ga^0X, the thermalization of the In^0X energy levels is very weak due to the very short In^0X lifetime (~3 ns). So, in magnetic fields of high (fig. 10) intensity one can clearly observe all the components (six groups of three/five peaks for the <111>/<001> & <110> directions). The same labelling scheme as for the Al acceptor was used to classify the PL peaks. Positions of the peaks versus magnetic field for the three main crystallographic axes and the results of the numerical simulation are shown on Fig. 11. Figure 4c shows schematically the expected evolution of the valley-orbit levels in magnetic field. The theoretical parameters are listed in Table 1.

Indium is the only acceptor in which we have detected the spin-orbit interaction, with the interaction constant λ=0.11 cm^{-1}.

4.4 Exciton bound to the Tl acceptor.

The Tl acceptor is the deepest amongst the group III acceptors. Since it's binding energy is comparable to the Si energy gap, approximately one quarter, Tl was considered to be a different type of impurity than the shallow group III acceptors. This perception was supported by the earlier studies of Tl^0X in PL and near-infrared absorption [33]. Elliot, McGill et. al resolved four peaks in the NP PL and absorption spectra. The VOS of the A^0X was neglected at this time and the widely accepted the *j-j* coupling model was not able to explain the

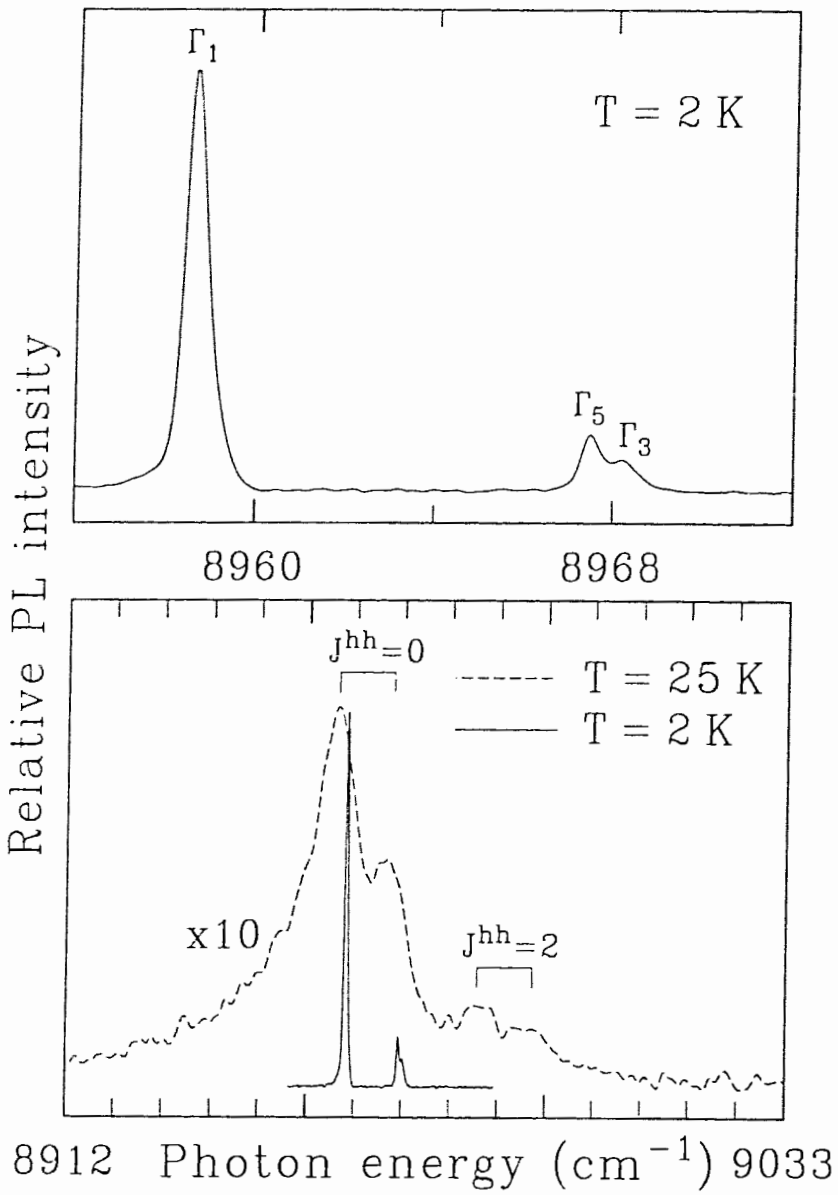

fig.12 The spectra of no-phonon PL of Tl^0X in zero magentic field at temperatures T=1.4K and T=25K

spectra. The essence of *j-j* coupling model is that the two-hole wavefunction for A^0X can be written as an antisymmetric product of the single-hole wavefunctions. In this case, the antisymmetric product $\{\Gamma_8 x \Gamma_8\}=\Gamma_1+\Gamma_3+\Gamma_5$. The Γ_1 state is associated with the $j^{hh}=0$ and the Γ_3 and Γ_5 states with the $j^{hh}=2$. In this work we demonstrate that the Tl^0X spectra can be explained in terms of the model developed for the shallow group III acceptors.

The previous Tl^0X spectrum by Elliot et al. can be explained if VOS is taken into account. Two higher energy transitions are associated with the $j^{h}=2$ state (see fig. 12). The other two states can be explained as the $j^{h}=0$ state is split further into Γ_1 and (Γ_3, Γ_5) states by taking into account the VOS in Tl^0X. Our analysis based on the stress and Zeeman effect measurements shows that the order of the VO states increasing in energy is Γ_1, Γ_5 and Γ_3 with the Γ_5 and Γ_3 states lying $8.9cm^{-1}$ and $9.6cm^{-1}$ higher then the Γ_1 state. The Γ_3 and Γ_5 states are present in the spectrum even at 2K ($8cm^{-1}$ ~ 14K) because the lifetime of Tl^0X is too short, and the inter-valley scattering is too slow for the VO states to thermalize. The Γ_1 and Γ_5 components undergo dramatic thermal broadening with increasing temperature up to 25K so the components can no longer be resolved and the resulting spectrum is very similar to one observed by Elliot et al. (see fig. 12).

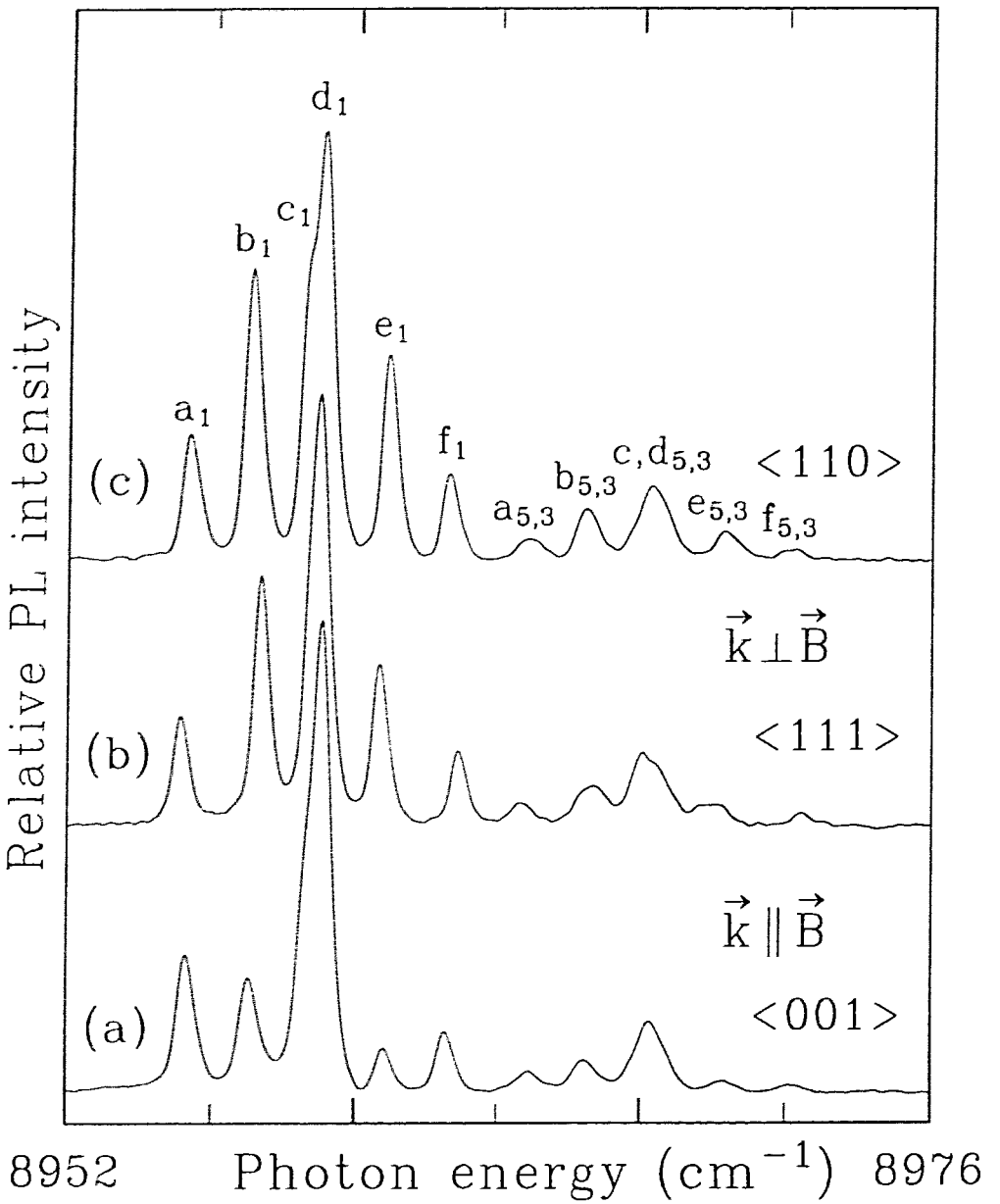

fig. 13 Si: Tl^0X PL spectra collected in Faraday and Voigt configurations at T=2K in magnetic field B=6T with a) <001>, b) <111> and c) <110> orientations

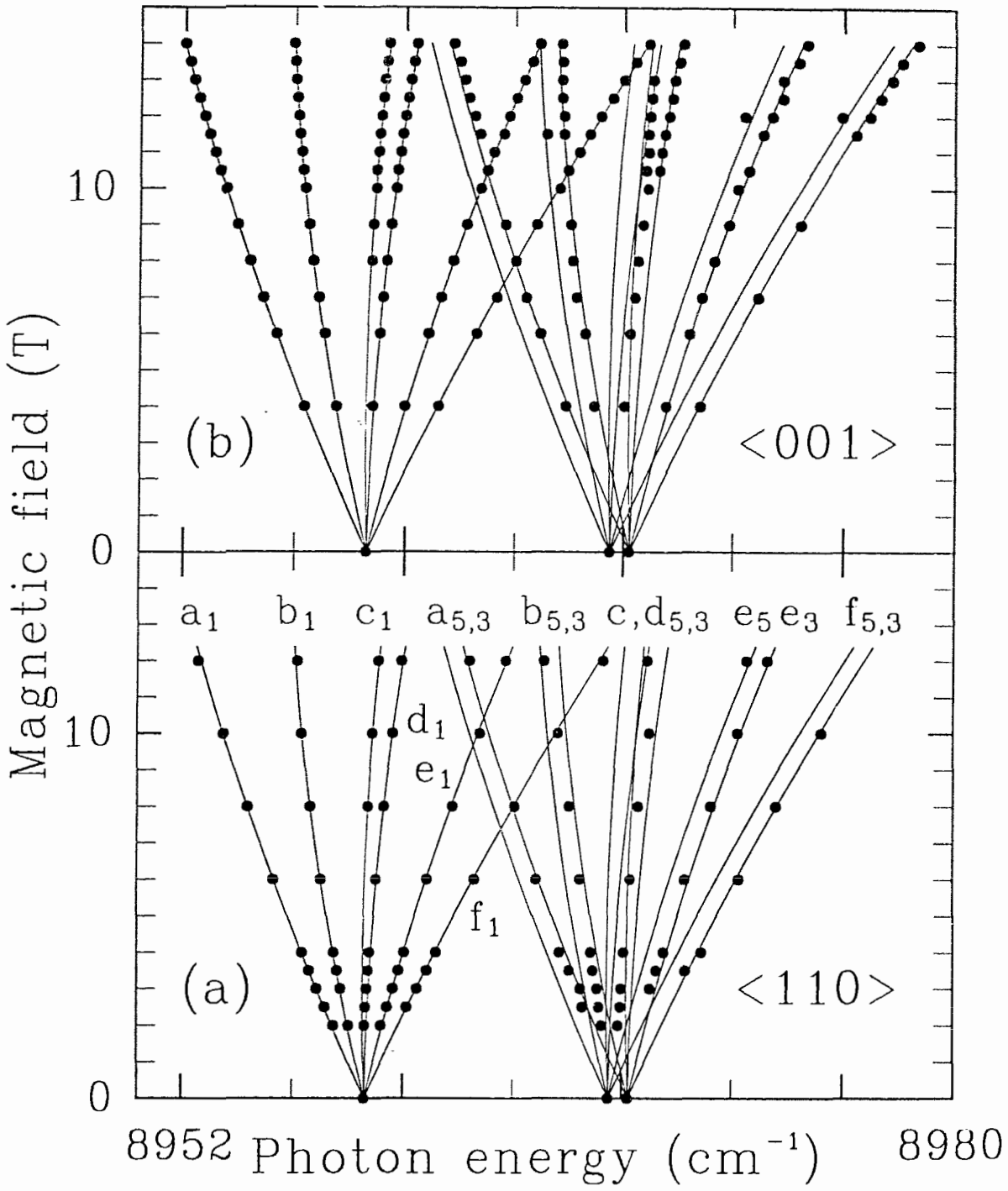

fig. 14 Si: Tl^0X Experimental (dots) and theoretical (solid lines) positions of PL spectra as a function of magnetic field with a) <110> and b) <001> orientations

As was mentioned, we have used the same principles for all the A^0X to label the PL peaks (see fig. 13) and to describe the evolution of the transition energies in magnetic fields. The parameters of the model listed in table 1 were found from the best fit between analytical solutions for the equations (13, 14, ref. 8) and experimental results (see fig. 14) for <001> and <111> directions in magnetic fields up to 14T.

The size of the VOS in Tl^0X is intermediate between the VOS in the other group III A^0X's and the VOS in shallow D^0X's. This indicates that Tl^0X can be described as a pseudodonor. The order of the VO states for Tl^0X is similar to the order of the VO states for D^0 and D^0X.

Chapter 5. Conclusion.

Studies of the Zeeman effect on excitons bound to Al, Ga and Tl neutral acceptors in silicon were performed using ultra high resolution Fourier-transform magnetospectroscopy in magnetic fields up to 14T at a temperature of 2K. Our results confirmed that in the ground state of A^0X the two holes from a spin singlet. We determined the values of the g-factors with high accuracy (within 1%). It is interesting to note that all g_1-factors are close to 1 for Al, Ga and In, which is the classical value for the gyromagnetic ratio. As the impurity becomes deeper the g_1-factors responsible for the cubical part of the wavefunction are decreasing and the g_2-factors reflecting the tetrahedral correction are growing. This is consistent with the perturbation theory; the further the energy levels are from the valence and conduction bands the larger the T_d correction. The diamagnetic shift constants q are proportional to the square of the effective radius and can be used to compare the effective radii of the A^0X for different impurities. From Table 1 it follows that the effective radius of the A^0 is decreasing but not as much as one would expect knowing the ionization energies (see table 1).

The splitting between the Γ_3 and Γ_5 VO states in A^0X is almost the same for all group III acceptors while the Γ_1 valley-orbit state becomes deeper as the ionization energy of A^0 increases (see fig. 15, table 1). This may be due to stronger localization of the holes in A^0X with larger A^0 ionization energy. Only in the In^0X was the spin-orbit interaction strong enough to be detected. The Γ_5

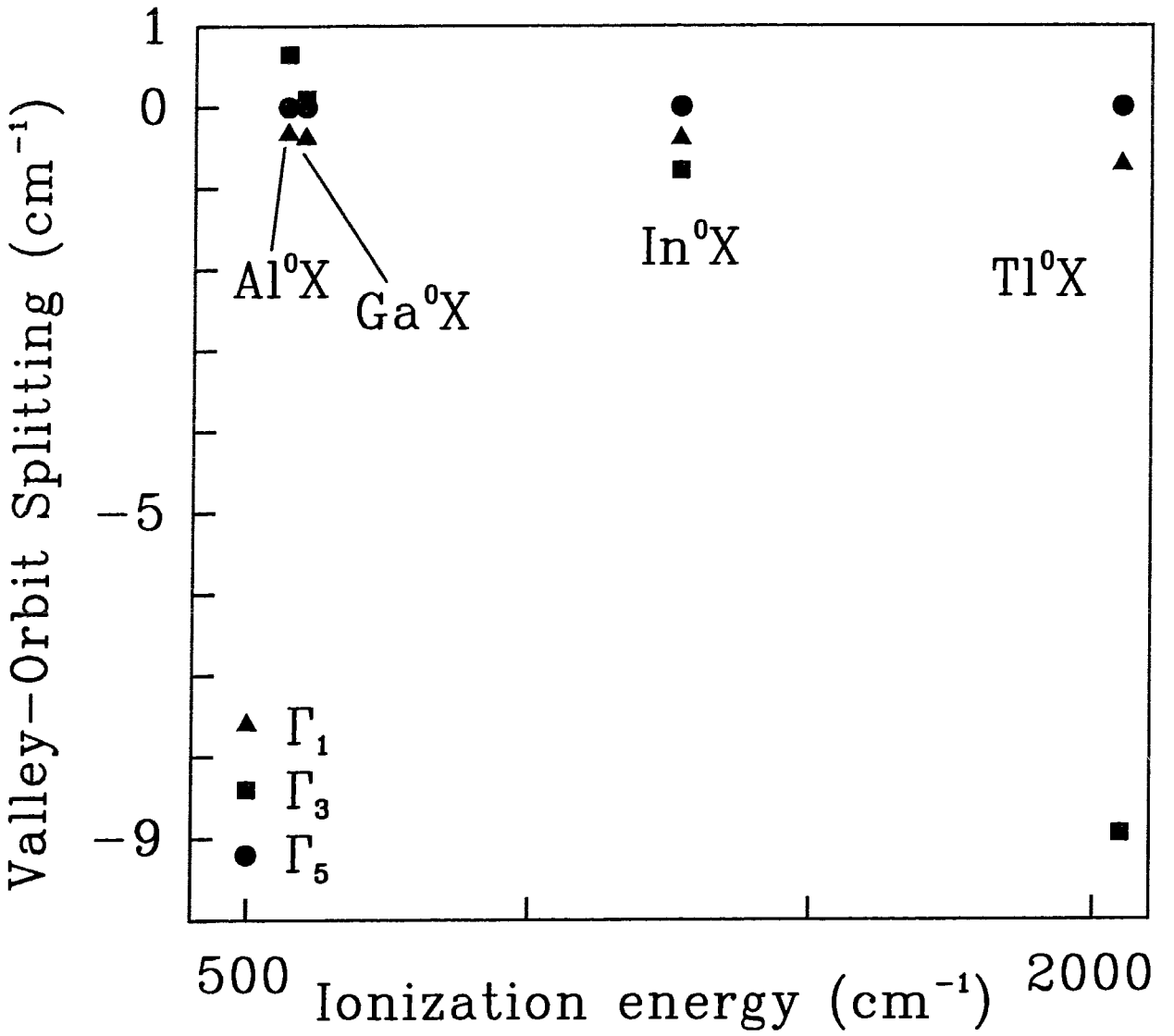

fig. 15 Valley-orbit splitting of different impurities as a function of impurity ionization energy. For all A^0X the position of the Γ_5 level was taken as the "zero" energy level. For In^0X the position of the Γ_5 level is defined as follows. The spin-orbit interaction splits the Γ_5 level (six degeneracy, including spin) into the lower energy level of double degeneracy and the higher energy level of quadruple degeneracy. Thus, to account for the degeneracy effect the position of Γ_5 level without spin-orbit interaction should be between two peaks at one third of the spin-orbit splitting from the higher energy level.

level in the In^0X is split by 0.16 cm^{-1} due to the spin-orbit coupling. This successful numerical simulation has proven the validity of the proposed model for A^0X. We have also found that the selection rules calculated theoretically by Kaminskii and *et al.* [22] are in agreement with the observed spectra.

	Al	Ga	In	Tl
$E^{I}_{ionization}(cm^{-1})$	566	597.21	1,265.4	1,984
g_1	0.98	0.96	0.86	0.6
g_2	-0.01	-0.01	-0.05	0.05
q_2 ($cm^{-1}T^{-2}$)	0.0009	0.0009	0.0024	0.0016
q_2+q_3($cm^{-1}T^{-2}$)	0.0007	0.0006	0.0023	0.0014
q_{sum} ($cm^{-1}T^{-2}$)	0.012	0.012	0.011	0.0095
$q^{e}_{II}-q^{e}_{per}$ ($cm^{-1}T^{-2}$)	0.18	0.01	0.012	n/a
$\Delta_1(\Gamma_1-\Gamma_5)(cm^{-1})$	0.67	0.1	-0.78	-8.95
$\Delta_2(\Gamma_3-\Gamma_5)(cm^{-1})$	-0.3	0.3	-0.38	0.72
spin-orbit(cm^{-1})	n/a	n/a	0.11	n/a

Table 1. The ionization energies, the parameters of the electronic valley-orbit splitting, the hole g-factors and the diamagnetic shift constants for various group III neutral acceptor bound excitons in Si. The q_{sum} represents the summary isotropic diamagnetic shift of the initial and final states.

REFERENCES:

1) M.L.W. Thewalt, in Excitons, edited by E.I. Rashba and M.D. Sturge (North-Holland, Amsterdam, 1982), p393

2) A.K. Ramdas, S. Rodriguez, 1981, Rep. Prog. Phys., vol. 44, p.1298

3) M.A. Lampert, 1958, Phys. Rev. Lett. 1, 450

4) J.R. Haynes, 1960, Phys. Rev. Lett. 4, 361

5) G. Kirczenow, Can. J. Phys., 1977, vol. 55, p.1787

6) A.S. Kaminskii, Ya. E. Pokrovskii, Teor. Fiz. Pis'ma Red. 11, 381, (1970)

7) G.L. Bir, G.E. Pikus, Symmetry and Strain Induced Effects in Semiconductors (Halsted, New York, 1974)

8) Anadi K. Bhattacharjee, S. Rodriguez, 1972, Phys. Rev. B, 6 (10), p.3836

9) V.A. Karasuyk, D.M. Brake, M.L.T. Thewalt, 1993, Phys. Rev. B,47 (15), p.9354

10) V. D. Kulakovskii, A.V. Malyavkin and V.B. Timofeev, 1979 Sov. Phys. JETP 49, 139

11) J. Weber, H. Conzelman and R. Sauer, in proceedings of the Fifteenth International Conference on the Physics of Semiconductors, Kyoto, 1980 [J. Phys. Soc. Jpn. Suppl. A 49, 425 (1980)]

12) E.U. Condon, G.H. Shortley, The theory of Atomic Spectra [Cambridge University Press, Cambridge, 1964]

13) P.J. Dean, D.C. Herbert, D. Bimberg and W.J. Choyke, Phys. Rev. Lett. 37, 1635 (1976)

14) D.C. Herbert, P.J. Dean, W.J. Choyke, Solid State Comm. 24, 383, (1977)

15) M.L.W. Thewalt Can. J. Phys. 55, 1463 (1977)

16) M.L.W. Thewalt Solid State Comm. 23, 733, (1977)

17) M.L.W. Thewalt and D.M. Brake, Materials Science Forum 65-66, 187 (1990)

18) R.R. Parsons, Solid State Commun., 22, 671 (1977)

19) A.S. Kaminskii, V.A. Karasuyk, Ya.E. Pokrovskii, JETP Lett. 33, 133 (1981)

20) A.S. Kaminskii, V.A. Karasuyk, Ya. E. Pokrovskii, Sov. Phys. JETP, 52, 211 (1980)

21) M.V. Gorbunov, A.S. Kaminskii, A.N. Safonov, Sov. Phys. JETP, 67, 355 (1988)

22) A.S. Kaminskii, V.A. Karasuyk, Ya.E. Pokrovskii, Sov. Phys. JETP, 56, 1295 (1983)

23) Peter R. Griffiths, James A. de Haseth, Fourier Transform Infrared Spectroscopy, *Series Chemical Analysis*, 1986

24) P.J. Dean, D.C. Herbert, D. Bimberg, W.J. Choyke, Phys. Rev. Lett. 37, 1635, (1976)

25) D.C.Herbert, P.J. Dean, W.J. Choyke Solid State Comm. 24, 383, (1977)

26) M.L.W. Thewalt Solid State Comm. 25, 513, (1978)

27) K. Kosai, M. Gershenzon Phys. Rev. B, 9, 723, 1974

28) R. Sauer Phys. Rev. Lett. 31, 376, 1973

29) R. Sauer, J. Weber Phys. Rev. Lett. 36, 48, 1976

30) B.P. Zakharchenya, I.B. Rusanov Opt. i Spectroskopia 19, 365 (1965) [Opt. Spectry. USSR, 19, 207, (1965)]

31) V.A. Karasuyk, S.An, M.L.W. Thewalt, Sol. Stat. Comm. 93(5), p.379, (1995)

32) N.O. Lipari, M.L.W. Thewalt J. Phys. Soc. Japan 49, Suppl. A, p.165, (1980)

33) K.R. Elliot, D.L. Smith, T.C. McGill. Sol. St. Comm. 27, 317 (1978)

34) L.D. Landau, E.M. Lifshitz, *Quantum Mechanics* (Pergamon Press, New York, 1976), p.429

35) V.A. Karasuyk and Ya.E.Pokrovskii, JETP Lett. 37 (11), p.640, (1983)

36) J.M. Luttinger, W. Koh, Phys. Rev. 97, 869 (1955)

37) J.M. Luttinger, Phys. Rev. 102(4), 1030 (1955)

38) V.A. Karasyuk, M.L.W. Thewalt, S. An, Phys. Rev. Lett.73(17), p.2340, (1994)

39) V.A. Karasuyk, et al., Phys. Rev. B 45(20), p.11736 (1992)

40) Landolt-Bornstein, *Numerical Data and Functional Relationships* in *Science and Technology, New Series*, group III, vol. 22, Semiconductors, subvolume b, editor in chief O. Msdelung, Springer-Verlag, Berlin (1989)

41) N.W. Ashcroft and N.D. Mermin, *Solid State Physics*, Holt, Rinehart and Winston, Inc., Philadelphia (1976)